*The Canadian Mineralogist*
Vol. 48, pp. 947-968 (2010)
DOI: 10.3749/canmin.48.4.947

# THE ORIGIN OF FERROAN-POTASSIC A-TYPE GRANITOIDS: THE CASE OF THE HORNBLENDE–BIOTITE GRANITE SUITE OF THE MESOPROTEROZOIC MAZURY COMPLEX, NORTHEASTERN POLAND

Jean-Clair DUCHESNE

*Département de Géologie, Université de Liège, Bât. B20, B–4000 Sart Tilman, Belgium*

Hervé MARTIN

*Laboratoire Magmas et Volcans, Université Blaise-Pascal, OPGC, CNRS, IRD, 5, rue Kessler, F–63038 Clermont Ferrand, France*

Bogusław BAGIŃSKI

*Institute of Geochemistry, Mineralogy and Petrology, Warsaw University, Żwirki i Wigury 93, PL–02-089 Warszawa, Poland*

Janina WISZNIEWSKA

*Polish Geological Institute, Rakowiecka 4, PL–00-975 Warszawa, Poland*

Jacqueline VANDER AUWERA

*Département de Géologie, Université de Liège, Bât. B20, B–4000 Sart Tilman, Belgium*

## Abstract

The mechanisms of differentiation and the source rocks of hornblende–biotite granitoids from the 1.5 Ga Mazury Complex, in the East European Craton in northeastern Poland, were investigated with major and trace elements and Sr–Nd isotopes on drill-core samples from six localities. The rock suites show metaluminous, ferroan, potassic and mostly alkali-calcic characters, together with high contents of incompatible elements typical of A-type granitoids. The presence of magnetite and a low Fe/(Fe + Mg) value of the hornblende indicate rather oxidized conditions of crystallization. In Harker diagrams, the major elements plot on a nearly continuous trend from 43 to 67 wt% $SiO_2$. From 56 wt% $SiO_2$ onward, the overall trend overlaps with the Tranevåg liquid line of descent, defined for hornblende–biotite granite in southern Norway. Most trace-element concentrations show decreasing trends with increasing $SiO_2$. The rare-earth-element concentrations are controlled by the apatite contents of the samples. The overall geochemical trend results from fractional crystallization and can be modeled by subtraction of mafic-mineral-rich cumulates. The suite is formed from melts at different degrees of fractionation, laden with various amounts of cumulus minerals. The initial $\varepsilon_{Nd}$ ranges from –3.3 to –6.8, with relatively low values of the initial Sr isotope ratio (0.702–0.707). Because of the absence of Archean rocks in this part of the East European Craton, most $\varepsilon_{Nd}$ negative values are consistent with melting of a juvenile crust extracted from the mantle at *ca*. 2.0–2.2 Ga. In the Mazury Complex, the parent magma for the 1.5 Ga Suwalki anorthosite was also formed by the melting of juvenile crust within the same time range. The Mazury batholith was emplaced along a linear zone of weakness, which facilitated melting of the lower crust. The melting products were a hornblende–biotite granite suite, oxidized and $H_2O$-rich, associated with an anorthosite–ferrodiorite suite, formed under dry and more reduced conditions. This is another line of evidence that, in anorthosite – mangerite – charnockite – granite (AMCG) complexes, two different crustal source-rocks can produce two different suites of rocks during the same melting episode.

*Keywords*: petrogenetic models, crustal source, Sr–Nd isotopes, East European Craton, rapakivi granite, AMCG suite, oxidized A-type granite, anorthosite, Mazury batholith, Poland.

§ *E-mail address*: jc.duchesne@ulg.ac.be

## Sommaire

Les mécanismes de différenciation et les roches sources des granitoïdes à hornblende et biotite du complexe de Mazury, faisant partie du craton Est Européen, en Pologne, d'âge 1.5 Ga, sont étudiés sur des carottes de forages provenant de six intrusions au moyen des compositions en éléments majeurs, en traces et en isotopes Sr–Nd. La suite de roches montre un caractère métalumineux, ferro-potassique, et principalement alcali-calcique, ainsi que des teneurs élevées en éléments incompatibles, typiques des granites de type A. La présence de magnétite et le faible rapport Fe/(Fe + Mg) de la hornblende indiquent des conditions de cristallisation plutôt oxydantes. Dans les diagrammes de Harker, les éléments majeurs se disposent sur une tendance quasi continue depuis 43% jusqu'à 67% en poids de $SiO_2$. A partir de 56% $SiO_2$, la tendance générale se superpose à la lignée de différentiation de Tranevåg, définie par les granites à biotite et à hornblende du sud de la Norvège. La plupart des concentrations en éléments en trace décroissent avec l'augmentation de la silice. Les teneurs en terres rares varient avec le contenu en apatite des échantillons. La tendance évolutive générale résulte d'une cristallisation fractionnée qui peut être modélisée par soustraction de cumulats riches en minéraux mafiques. La suite de roches est constituée de liquides magmatiques à différents degrés de fractionnement et chargés de quantités variables de minéraux cumulés. La valeur du $\varepsilon_{Nd}$ initial va de –3.3 à –6.8, avec des rapports isotopiques initiaux du Sr faibles (0.702–0.707). Comme les roches archéennes sont absentes dans cette partie du craton Est Européen, la plupart des valeurs négatives de $\varepsilon_{Nd}$ peuvent s'expliquer par la fusion d'une croûte juvénile extraite du manteau *ca.* 2.0–2.2 Ga. Dans le complexe de Mazury, le magma parent de l'anorthosite de Suwalki (1.5 Ga) a aussi été formé par fusion d'une croûte juvénile dans ce même intervalle de temps. Le batholithe de Mazury s'est mis en place dans une zone linéaire de faiblesse, laquelle a facilité la fusion de la croûte inférieure. Les produits de cette fusion ont constitué la suite oxydée et riche en $H_2O$ des granites à hornblende et à biotite, ainsi que la suite anorthosite–ferrodiorite formée dans des conditions anhydres et réduites. Ce cas d'étude constitue un autre indice que dans les complexes anorthosite – mangérite – charnockite – granite (AMCG), deux sources crustales différentes peuvent produire deux suites différentes de roches au cours du même épisode de fusion.


*Mots-clés*: modèles pétrogénétiques, granite, source crustale, isotopes Sr–Nd, craton Est Européen, granite rapakivi, suite AMCG, granite de type A oxydé, anorthosite, batholite de Mazury, Pologne.

## Introduction

Plutonic suites involving anorthosites and rapakivi granites or anorthosite – mangerite – charnockite – (rapakivi) granite (AMCG) are typical constituents of Proterozoic crystalline domains (Emslie 1991, Rämö & Haapala 1995). The felsic members of the suite are characterized by high contents of potassium (>5 wt% $K_2O$) and Fe* [= FeOt/(FeOt + MgO)] values higher than 0.75, as well as high contents of incompatible elements (LILE: large-ion lithophile elements; REE: rare-earth elements; HFSE: high field-strength elements), typical of A-type granites. Such features are also shared by Proterozoic granites not spatially associated with anorthosites but emplaced within the same period of time. Classic examples are the 1.6–1.3 Ga A-type Laurentian granites (*e.g.,* Anderson & Morrison 2005, Goodge & Vervoort 2006), the 1.9–0.9 Ga anorogenic Amazonian granites (Dall'Agnol *et al.* 1994, Rämö *et al.* 2002), and the 1.0–0.9 Ga A-type Sveconorwegian granites of southern Norway (*e.g.*, Vander Auwera *et al.* 2003). Their occurrences result from specific mechanisms of differentiation, melting processes and source-rock variety in various tectonic settings (*e.g.,* Anderson & Bender 1989, Hoffman 1989, Ashwal 1993, Duchesne *et al.* 1999, Bogdanova *et al.* 2004, Vigneresse 2007). They are thus of utmost interest to decipher the characteristics of the evolution of the Proterozoic continental crust.

Anderson & Morrison (2005) proposed that the Mesoproterozoic A-type granites belong to two different series. The first one contains ilmenite and thus crystallized under reduced conditions; ilmenite typically prevails in igneous rocks associated with anorthosites. The reduced (ilmenite-bearing) series can be derived from mafic sources and granites produced by various processes, for example differentiation of a dry ferroan parental magma or partial melting of underplated basalts (the so-called tholeiitic connection of Frost & Frost 1997), or fractionation of a jotunitic (orthopyroxene monzodioritic) parental magma (Duchesne 1990, Vander Auwera *et al.* 1998b), generated by melting of a mafic lower continental crust (Longhi *et al.* 1999, Longhi 2005). The second suite contains magnetite and forms hornblende–biotite granites (HBG) under more oxidized conditions. Experimental evidence has shown that the high Fe* content of the magnetite series reflects relatively oxidized conditions of formation, provided the magma has a high content of $H_2O$ (up to 5–6 wt%) (Dall'Agnol *et al.* 1999, Bogaerts *et al.* 2006). Frost *et al.* (2002), however, considered that high values of oxygen fugacity are linked to high degrees of contamination. Obviously, a variety of source rocks and processes are required to produce the magmas that resulted in ferroan granites, and this in turn weakens the links to the geodynamic settings in which they are generated.

The Mazury Complex in northeastern Poland contains a wide variety of granite intrusions (Claesson *et al.* 1995, Baginski *et al.* 2001a, 2007, Skridlaite *et al.* 2003). The purpose of this paper is to investigate the major and trace elements as well as the Sr–Nd isotopic compositions of several hornblende–biotite granites (HBG) in order to decipher their differentiation

mechanisms and conditions of formation. A comparison with a similar well-documented HBG suite from South Norway and contemporaneous with the Rogaland anorthosite (Bogaerts *et al*. 2003, Vander Auwera *et al*. 2003, 2008) allows us to define a differentiation model for the Mazury HBG series. We identify fractional crystallization as the main mechanism of differentiation of the HBG oxidized melts and show that the rocks represent crystallized liquids laden with various proportions of cumulus minerals. The rocks show a restricted range of Nd and Sr isotope ratios at the time of intrusion and support an origin by melting a juvenile crustal material extracted from the mantle at *ca*. 2.1 Ga. As in South Norway, HBG oxidized granites are contemporaneous with anorthosite and ferrodiorite formed under reduced conditions, which suggests that different source-rocks can be melted during the same igeous event. As in several other AMCG complexes, the Mazury batholith was emplaced along a major linear tectonic structure.

## Geological Framework

The Mazury Complex, situated in northeastern Poland, is part of the East European Craton that forms the northeastern part of Europe (Fig. 1). It is covered by Phanerozoic platform sediments whose thickness varies from 400 m in the east to 5000 m at the edge of TESZ (TransEuropean Suture Zone). The crystalline basement is only known through geophysical investigations and drilling (Ryka & Podemski 1998). The Mazury Complex extends from Olsztyn in the West to the Veisiejai Complex in Lithuania in the East (Skridlaite *et al*. 2003). It is associated with three massifs of anorthosites (Kętrzyn, Suwałki and Sejny) and related rocks (Kubicki & Ryka 1982, Juskowiak 1998, Ryka & Podemski 1998, Wiszniewska *et al*. 2002). Combined geophysical approaches have been used to determine the shape, structure and extension of the Mazury magmatic belt (Wiszniewska *et al*. 2000) (Fig. 1). On the magnetic image map (not shown), the Mazury Complex consists of a mosaic of positive anomalies, whereas on a Bouguer anomaly map (Fig. 1a), the granitoids mostly show values higher than those of the anorthosite–norite massifs. The Mazury Complex intruded granulite-facies metamorphic rocks belonging to the West Lithuanian Domain and its southern Polish extension; the latter formed in Paleoproterozoic times and accreted at *ca*. 1.85–1.80 Ga (Bogdanova 1999, Bogdanova *et al*. 2006). The elongate structure of the Mazury Complex follows an E–W-trending shear zone that was repeatedly active for approximately 15 million years (1.6–1.45 Ga; Bogdanova *et al*. 2006). The structural setting of emplacement of the Mazury Complex is considered to be anorogenic (*e.g*., Dörr *et al*. 2002) or post-collisional (Skridlaite *et al*. 2003). Bogdanova *et al*. (2006) suggested a relationship between the metamorphic imprint in mylonites along major shear-zones and the AMCG magmatism.

The ages of crystallization of the Mazury Complex are relatively well constrained. Two zircon fractions extracted from the Gołdap and Bartoszyce boreholes in the Mazury granites give single-grain U–Pb ages of about 1.5 Ga (Claesson *et al*. 1995) Granites from four boreholes in the Mazury Complex (including Bartoszyce and Gołdap) give U–Pb zircon (TIMS) ages in the 1526–1499 Ma range on single crystals of zircon (Dörr *et al*. 2002). Also, Re–Os isochrons on sulfides (pyrrhotite, chalcopyrite and pyrite) and magnetite from the Suwałki anorthosite (Morgan *et al*. 2000) give ages of 1559 ± 37 and 1556 ± 94 Ma, respectively, which correspond within error to the granite ages. Some Mazury granitoids have depleted mantle Nd model ages ($T_{DM}$) of 2.1 to 2.2 Ga (Claesson *et al*. 1995), whereas the Suwałki anorthosite–gabbronorite complex yields Nd model ages of 2.0 to 2.3 Ga (Wiszniewska *et al*. 2002). About 100 km to the north of the Mazury Complex, another E–W-trending lineament (not shown in Fig. 1) is intruded by the Nemunas and Geluva AMCG granites, which have been dated by secondary ion mass spectrometry at 1447 ± 5 Ma and 1445 ± 8 Ma, respectively (Skridlaite *et al*. 2007).

## Analytical Methods

Analyses of the main rock-forming minerals were carried out on selected thin sections with a Cameca SX–100 electron-probe microanalyzer at the Electron Microprobe Laboratory of the Inter-Institute Analytical Complex for Minerals and Synthetic Substances at the Institute of Geochemistry, Mineralogy and Petrology, Warsaw University. We employed an acceleration voltage of 20 kV, a beam current of 10–20 nA, and a beam-spot diameter of 2 μm. We used natural and artificial substances as standards and the PAP program (Pouchou & Pichoir 1991) for corrections.

We analyzed samples from the six boreholes (Appendix 1) for major elements, Rb and Sr with a Philips PW 2400 Rtg spectrometer at the Central Laboratory of the Polish Geological Institute. Concentrations of the major elements were established using standard X-ray fluorescence (XRF) fusion techniques. The precision and accuracy of these determinations generally were found to be better than 5%. Concentrations of the REE, Y, Zr, Nb, Ba, V, Zn, Co, Cu, Ga, and Pb were established with the ICP–MS method with a VG elemental PQ 2 Plus spectrometer at the Université de Liège (Belgium), following the method described in Vander Auwera *et al*. (1998a).

Concentrations of Sm, Sr and Nd and whole-rock isotopic ratios were measured with a VG ISOMASS 54E mass spectrometer in the Laboratoire Magmas et Volcans, Clermont Ferrand, France. A CAMECA TSN 206 solid-source mass spectrometer was used to

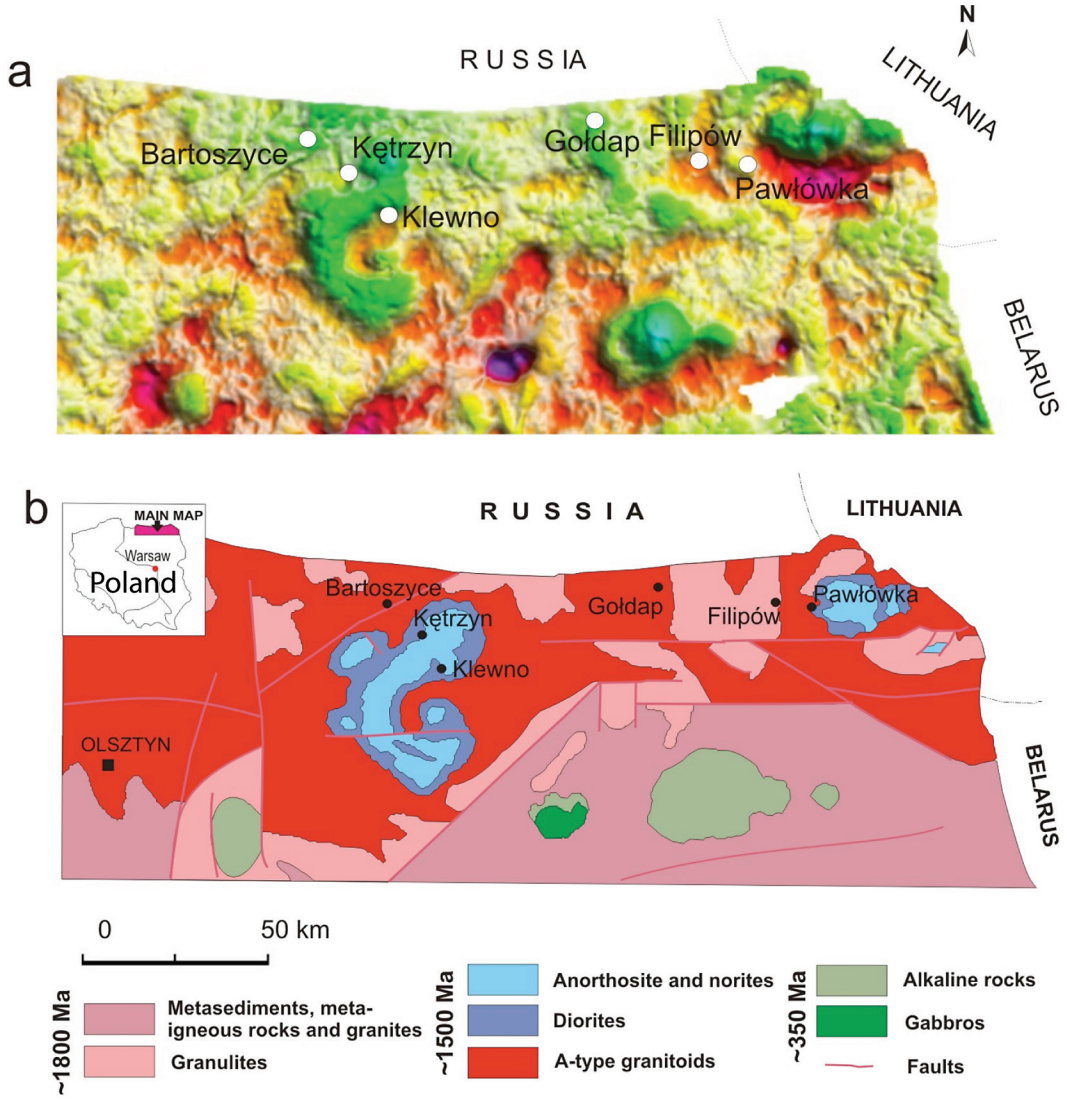


FIG. 1. a. Gravity map of northern Poland (Bouguer anomaly, transformed) outlining the major geological structures presented on Figure1b (from Wybraniec 2007, unpublished), and the location of the boreholes studied. b. Simplified geological map of northern Poland (after Kubicki & Ryka 1982, modified) with the location of the boreholes studied.

measure Rb contents. The $^{87}Sr/^{86}Sr$ values were normalized to $^{86}Sr/^{88}Sr = 0.1194$, and the $^{143}Nd/^{144}Nd$ values to $^{146}Nd/^{144}Nd = 0.7219$. Relative uncertainties for $^{147}Sm/^{144}Nd$ and $^{87}Rb/^{86}Sr$ are 0.5% and 2%, respectively. The Nd isotopic values were normalized to a La Jolla standard value of 0.511860. The $T_{DM}$ ages were calculated using the present-day depleted mantle values of $^{143}Nd/^{144}Nd = 0.51315$ ($\varepsilon_o = +10$) and $^{147}Sm/^{144}Nd = 0.2137$, following a radiogenic linear growth for the mantle with $\varepsilon_{Nd} = 0$ at 4.55 Ga.

## PETROLOGY

Drill cores from Klewno, Kętrzyn, Bartoszyce, Filipów, Pawłówka, and Gołdap (Fig. 1) intrusions were investigated in this study. Detailed petrographic descriptions can be found in Baginski *et al.* (2001b). The rocks range from diorite (Klewno) to granodiorite and monzogranite (Gołdap) and present a similar mineralogy and texture. They are medium to coarse grained, with porphyritic plagioclase and K-feldspar (up to 3

cm long). The matrix typically contains plagioclase and K-feldspar together with hornblende and biotite as major constituents, as well as subordinate amounts of quartz and clinopyroxene. The latter shows evidence for reaction to hornblende, except in Klewno and Gołdap, where it is absent. Apatite, titanite, zircon, magnetite and ilmenite are the main accessory phases. Quartz is present in the most evolved rocks, and myrmekite and biotite–quartz symplectites are common. Rapakivi textures were locally observed in a small number of samples. The mineralogy and texture of this suite of granitic rocks are very similar to what is observed in the HBG suite emplaced at the end of the Sveconorwegian orogeny in southern Norway (Vander Auwera *et al*. 2003, 2008).

The mineral compositions of these granitic rocks are summarized in Table 1. Plagioclase is weakly zoned andesine, and the K-feldspar is perthitic orthoclase. Amphibole compositions (Table 2) range from edenite in Klewno to magnesium hastingsitic hornblende in Gołdap (Fig. 2). Application of the amphibole geobarometers of Johnson & Rutherford (1989) and Schmidt (1992) gives pressures of 2–3 kbar for Klewno and 4–5 kbar for the other massifs. The biotite consists of high-Ti and high-F annite (up to 4.8 wt% $TiO_2$ and 2.3 wt% F in Bartoszyce). Titanite locally rims ilmenite grains. The An content in plagioclase is negatively correlated with the $SiO_2$ content of the host rock, whereas the fe# value [=100*FeOt/(FeOt+MgO)] of hornblende, biotite and clinopyroxene (where present) increases. An exception is in the Kętrzyn pluton, where at similar An contents, the fe# of hornblende and biotite are much higher than in the other occurrences, with values of 50 and 43, respectively (Tables 1, 2). This may reflect more reduced conditions of crystallization, which favored the incorporation of $Fe^{2+}$ in mafic minerals, whereas, under more oxidized conditions, Fe is partly oxidized to $Fe^{3+}$ and enters early-formed magnetite (Toplis & Carroll 1995, Bogaerts *et al*. 2006). The Kętrzyn granitoids are spatially related to anorthosites and related rocks (in Fig. 1, the borehole is located in the Kętrzyn anorthosite), a rock series that has crystallized under more reduced conditions than the HBG suite (Frost & Frost 1997, Vander Auwera *et al*. 2003, 2008, Bogaerts *et al*. 2006)

TABLE 1. RANGE OF MINERAL COMPOSITIONS OBSERVED IN A SELECTION OF SAMPLES FROM THE MAZURY COMPLEX

| Sample # | $SiO_2$% range | Pl An% | fe# hbl | fe# bt | fe# cpx | $SiO_2$% melt |
|---|---|---|---|---|---|---|
| Klewno 2 | 46-51 | 40-37 [4] | 31 (2) [5] | 30 (2) [3] | 28 (1) [4] | 56 |
| Ketrzyn 3 | 53-59 | 34-28 [11] | 50 (0) [4] | 43 (0) [4] | absent | 59 |
| Bartoscyce 6 | 51-63 | 34-31 [4] | 38 (2) [4] | 27 (4) [3] | 32 (1) [4] | 63 |
| Bartoscyce 4 | 51-63 | 32-30 [9] | 37 (1) [8] | 28 (2) [18] | 32 (2) (3] | 63 |
| Goldap 3 | 63-66 | 30-26 [7] | 43 (1) [9] | 29 (1) [9] | absent | 66 |

$SiO_2$% range: range of values in the occurrence. $SiO_2$% melt: estimated melt composition (no accumulated minerals) (see text). fe#: 100Fe/(Fe + Mg). In brackets, standard deviation of the value; in square brackets, number of analyses. Compositions were established by electron-microprobe analysis.

## Geochemistry

The compositions of the rocks in terms of major and trace elements are reported in Table 3 and displayed in Figures 3, 4 and 5.

### *Major elements*

The Klewno samples have the lowest $SiO_2$ (46.6 wt%) and $K_2O$ (2.6%) contents, and the highest FeOt (up to 14.9%), MgO (3.9%), $TiO_2$ (2.9%), and $P_2O_5$ (2.2%) contents, whereas the Gołdap massif displays the most differentiated and evolved rocks. In Harker diagrams (Fig. 3), samples from the various massifs form continuous trends, with little or no overlap. The rocks are metaluminous; the modified alkali–lime index of Frost *et al*. (2001), MALI, varies from –1.05 to 7.92, and Fe* ranges from 0.75 to 0.85, which demonstrates the alkali-calcic and ferroan characters. In a $K_2O$ *versus* $SiO_2$ diagram (Fig. 3), most samples plot in the shoshonitic field, whereas only few display high-K affinities. An AFM diagram indicates amazingly constant and high FeOt/MgO values (Fig. 4). In Figure 3, the composition of the Mazury granitoids is also compared to that of

TABLE 2. AVERAGE COMPOSITIONS OF AMPHIBOLE FROM THE MAZURY GRANITOID INTRUSIONS

| | KW2 | K3 | B4 | B6 | G3 |
|---|---|---|---|---|---|
| *n* | 5 | 4 | 8 | 4 | 9 |
| $SiO_2$ wt% | 47.40 | 42.91 | 44.12 | 43.66 | 43.26 |
| $TiO_2$ | 0.77 | 1.37 | 1.31 | 1.47 | 1.20 |
| $Al_2O_3$ | 7.51 | 9.39 | 9.50 | 9.37 | 9.74 |
| FeO | 12.21 | 17.71 | 13.72 | 14.26 | 15.62 |
| MnO | 0.48 | 0.81 | 0.59 | 0.52 | 0.93 |
| MgO | 15.16 | 9.84 | 12.93 | 12.81 | 11.85 |
| CaO | 11.71 | 11.42 | 11.77 | 11.35 | 11.63 |
| $Na_2O$ | 1.22 | 1.51 | 1.68 | 1.70 | 1.79 |
| $K_2O$ | 0.88 | 1.39 | 1.49 | 1.50 | 1.56 |
| $H_2O$ | 2.04 | 1.95 | 2.00 | 1.98 | 1.99 |
| Total | 99.38 | 98.31 | 99.11 | 98.62 | 99.59 |
| Si *apfu* | 6.954 | 6.613 | 6.613 | 6.594 | 6.534 |
| Ti | 0.086 | 0.159 | 0.147 | 0.168 | 0.136 |
| Al | 1.298 | 1.706 | 1.678 | 1.668 | 1.734 |
| Fe | 1.500 | 2.282 | 1.721 | 1.802 | 1.973 |
| Mn | 0.060 | 0.106 | 0.075 | 0.067 | 0.119 |
| Mg | 3.312 | 2.261 | 2.889 | 2.882 | 2.668 |
| Ca | 1.840 | 1.886 | 1.891 | 1.835 | 1.882 |
| Na | 0.344 | 0.453 | 0.488 | 0.498 | 0.523 |
| K | 0.166 | 0.273 | 0.284 | 0.288 | 0.300 |
| $^{IV}$Al | 1.16 | 1.45 | 1.45 | 1.50 | 1.55 |
| Fe/(Fe + Mg) | 0.31 | 0.50 | 0.37 | 0.38 | 0.43 |

Electron-microprobe data; *n* is the number of analyses.

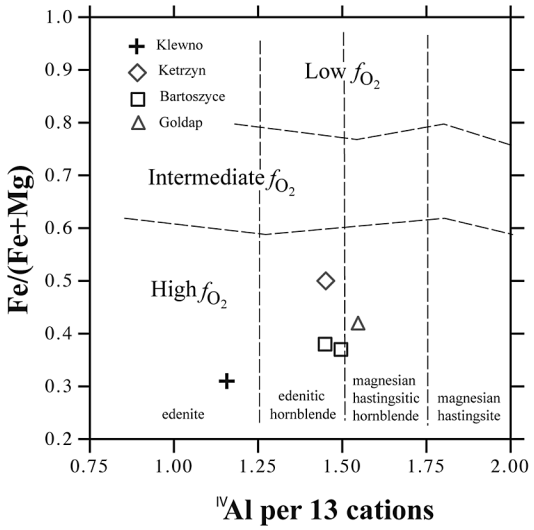


FIG. 2. Fe/(Fe + Mg) *versus* $^{IV}$Al in average amphiboles showing the oxidized conditions of crystallization. Nomenclature after Leake *et al*. (1997). The dividing lines are from Rämö *et al*. (2002).

the south Norwegian HBG suite. For this comparison, geochemical data obtained on the Tranevåg intrusion, associated with the Lyngdal granodiorite (southern Norway), have been selected (Bogaerts *et al*. 2003, Vander Auwera *et al*. 2003). From its starting composition at 56% up to 69% $SiO_2$, the Tranevåg trend indeed almost perfectly coincides with the Mazury trend for FeOt, MgO, CaO, $TiO_2$ and $Na_2O$, and is slightly below it for $Al_2O_3$ and $K_2O$.

*Trace elements*

The Zr, Nb and REE concentrations (Fig. 5) are relatively high and typical of A-type granites (Whalen *et al*. 1987) (Fig. 6), as is also the HBG suite (Bogaerts *et al*. 2003, Vander Auwera *et al*. 2003). As observed for the major elements, concentrations of trace elements, if plotted against $SiO_2$, show loosely defined trends (Fig. 5). All elements are inversely correlated with $SiO_2$, except Rb and Pb, which are positively correlated, and Ba, which is roughly constant. In these diagrams, the trace elements show some scatter, which results in differentiation trends that are less well defined than for major elements. Diagrams of CaO *versus* $P_2O_5$ as well as Ce *versus* $P_2O_5$ (Fig. 7) show that both CaO and Ce are positively correlated with $P_2O_5$, which results from the important role played by apatite in the whole-rock composition. The light REE concentrations (ppm) are very high (56 < La < 265), whereas the heavy REE are also moderately high (3 < Yb < 9.4), which results in regularly fractionated patterns, $(La/Yb)_N$ =15 ± 2, except for the Klewno samples, where $(La/Yb)_N$ ranges from 25 to 30 (Fig. 8, Table 3). Most samples also show a small negative anomaly (0.53 < Eu/Eu* < 0.96, with an average at 0.75 ± 0.10, Table 3). The small $(La/Yb)_N$ ratios and Eu anomalies obviously reflect the control of apatite over the REE contents.

Some trace elements show distinctive behaviors (Fig. 5): (1) Sr concentrations appear to remain constant within each massif, but change from massif to massif, showing a general inverse correlation with silica content; (2) Zn, V and Co concentrations decrease with differentiation (see below, Fig. 9); (3) Zr shows a similar evolution with the exception of most Klewno samples, which have significantly lower Zr contents, and (4) Nb concentrations are relatively scattered; however, within each individual massif, Nb is gently negatively correlated with $SiO_2$. As for the major elements, comparison with the Tranevåg series (Fig. 5) shows great similarities in the behavior of all trace elements, except that Rb and Pb are less incompatible in the Tranevåg suite.

*Radiogenic isotopes*

The Sr and Nd isotopic compositions of seven samples from the various massifs are shown in Table 4 and in Figures 10–12. The $\varepsilon_{Nd}$ values calculated at the age of crystallization (1.5 Ga) range from –3.3 (Klewno) to –6.8 (Pawłówka), whereas the initial $^{87}Sr/^{86}Sr$ values extend from 0.702 (Gołdap) to 0.707 (Filipów). The $T_{DM}$ model ages (DePaolo 1983) range from 2.4 Ga (Pawłówka) to 2.0 Ga (Klewno) with all values, except Klewno (2.04 Ga), averaging at 2.18 ± 0.03 Ga.

## DISCUSSION

*The HBG suite belongs to the oxidized A-type granite series*

The 1.5 Ga Mazury HBG felsic rocks show typical characteristics of Proterozoic A-type granites (*e.g.*, Whalen *et al*. 1987), *i.e.*, metaluminous and ferroan whole-rock compositions with high $K_2O$ and incompatible elements contents. The occurrence of magnetite in the mineral association and the low Fe/(Fe+Mg) value of the hornblende indicate oxidized conditions of crystallization (Dall'Agnol *et al*. 1999, Anderson & Morrison 2005). The Mazury HBG suite is very similar, in mineralogy and composition, to the south Norwegian Tranevåg A-type granite (Fig. 3), which derives from a hydrated parental magma of intermediate composition (Bogaerts *et al*. 2003, 2006). This similarity allows us to investigate the Mazury rocks in light of the petrogenetic model developed for the Tranevåg series, as is done below.

*Identification of the differentiation process*

In the Harker plot for $K_2O$ (Fig. 3) as well as in the CaO *versus* $P_2O_5$ diagram (Fig. 7), the points for the Mazury massifs clearly define broken or curved trends, which preclude any simple mixing process between two components, but rather suggests a process such as partial melting or fractional crystallization. In

TABLE 3a. MAJOR- AND TRACE-ELEMENT COMPOSITION OF SAMPLES FROM BOREHOLES IN THE MAZURY COMPLEX

| | Ketrzyn | | | | | | Pawlowka | | Bartoszyce | | | | | | |
|---|---|---|---|---|---|---|---|---|---|---|---|---|---|---|---|
| | K1 | K3 | K4 | K5 | K6 | K7 | P17 | P144 | B1 | B2 | B3 | B4 | B5 | B6 | B7 |
| $SiO_2$ wt% | 59.35 | 54.00 | 56.64 | 54.32 | 54.01 | 59.64 | 61.74 | 60.60 | 61.58 | 61.00 | 62.11 | 60.53 | 60.85 | 51.32 | 61.84 |
| $TiO_2$ | 1.04 | 1.86 | 1.45 | 1.79 | 1.82 | 1.38 | 1.55 | 1.68 | 1.22 | 1.30 | 0.93 | 1.37 | 1.21 | 2.22 | 0.99 |
| $Al_2O_3$ | 17.72 | 17.17 | 17.10 | 17.08 | 16.63 | 16.73 | 14.15 | 13.91 | 15.62 | 15.80 | 17.05 | 16.01 | 15.99 | 14.66 | 16.91 |
| $Fe_2O_3$t | 5.64 | 9.27 | 8.24 | 9.44 | 9.93 | 7.04 | 8.93 | 10.00 | 7.21 | 7.07 | 5.21 | 7.29 | 7.11 | 14.83 | 5.53 |
| MnO | 0.10 | 0.15 | 0.13 | 0.15 | 0.15 | 0.13 | 0.13 | 0.17 | 0.12 | 0.17 | 0.10 | 0.14 | 0.12 | 0.23 | 0.10 |
| MgO | 1.66 | 1.92 | 1.86 | 2.11 | 1.93 | 1.58 | 2.04 | 2.28 | 1.43 | 1.48 | 1.19 | 1.63 | 1.48 | 2.42 | 1.15 |
| CaO | 4.04 | 6.53 | 5.79 | 6.45 | 6.45 | 4.98 | 4.16 | 4.50 | 3.93 | 3.93 | 4.19 | 4.86 | 4.35 | 6.01 | 4.17 |
| NaO | 3.19 | 3.78 | 3.70 | 3.77 | 3.58 | 3.74 | 2.63 | 2.79 | 3.16 | 3.27 | 3.82 | 3.71 | 3.37 | 3.19 | 3.81 |
| $K_2O$ | 6.58 | 3.97 | 4.01 | 3.65 | 4.13 | 3.99 | 4.12 | 3.46 | 5.04 | 5.26 | 4.87 | 3.73 | 4.81 | 3.83 | 4.96 |
| $P_2O_5$ | 0.69 | 1.36 | 1.08 | 1.24 | 1.39 | 0.78 | 0.54 | 0.62 | 0.68 | 0.71 | 0.52 | 0.73 | 0.71 | 1.29 | 0.54 |
| Th ppm | 9 | 27 | 11 | 12 | 15 | 3 | 23 | 16 | | | | 5 | 5 | 8 | 4 |
| Zr | 659 | 1017 | 902 | 1010 | 1181 | 1290 | 504 | 572 | 784 | 771 | 546 | 632 | 763 | 1316 | 552 |
| Nb | 16 | 26 | 18 | 24 | 26 | 27 | 22 | 24 | 17 | 22 | 12 | 20 | 15 | 33 | 15 |
| Rb | 175 | 102 | 109 | 97 | 105 | 78 | 157 | 146 | 134 | 139 | 125 | 108 | 129 | 117 | 130 |
| Sr | 561 | 546 | 530 | 528 | 529 | 457 | 274 | 262 | 422 | 413 | 455 | 409 | 433 | 370 | 457 |
| Ba | 3509 | 2235 | 2228 | 2042 | 2431 | 2366 | 1322 | 1083 | 2280 | 2310 | 2118 | 1679 | 2164 | 1673 | 2193 |
| V | 66 | 122 | 111 | 120 | 132 | | 134 | 155 | 79 | 81 | 44 | 87 | 78 | 168 | 66 |
| Zn | 128 | 172 | 170 | 184 | 182 | 134 | 122 | 173 | 141 | 146 | 102 | 147 | 140 | 240 | 113 |
| Co | 10 | 15 | 13 | 14 | 14 | 14 | 17 | 17 | 3 | 8 | 3 | 3 | 3 | 7 | 6 |
| Cu | 5 | 11 | 7 | 14 | 13 | 15 | 22 | 21 | 10 | 10 | 10 | 10 | 10 | 10 | 10 |
| Ga | 23 | 26 | 25 | 27 | 26 | | 22 | 23 | 23 | 23 | 26 | 26 | 24 | 27 | 25 |
| Pb | 26 | 20 | 20 | 20 | 18 | | 30 | 31 | 32 | 35 | 32 | 29 | 33 | 24 | 35 |
| Y | 52 | 96 | 69 | 85 | 95 | | 52 | 62 | 46 | 49 | 38 | 52 | 51 | 102 | 35 |
| La | 102 | 235 | 133 | 155 | 190 | 136 | 114 | 93 | | | | 142 | 134 | 198 | 110 |
| Ce | 225 | 518 | 293 | 351 | 425 | 286 | 214 | 187 | | | | 291 | 271 | 432 | 227 |
| Pr | | | | | | | 24 | 22 | | | | 36 | 33 | 56 | 27 |
| Nd | 111 | 242 | 144 | 178 | 205 | 152 | 96 | 84 | | | | 137 | 154 | 219 | 105 |
| Sm | 21 | 40 | 25 | 32 | 36 | 26 | 17 | 16 | | | | 24 | 22 | 41 | 17 |
| Eu | 5.0 | 8.3 | 5.8 | 6.5 | 7.8 | 5.6 | 3.6 | 3.5 | | | | 4.7 | 4.5 | 5.8 | 4.6 |
| Gd | 15.7 | 28.4 | 20.3 | 24.8 | 26.3 | 18.6 | 13.0 | 12.6 | | | | 15.0 | 15.4 | 27.8 | 13.1 |
| Tb | 2.4 | 4.0 | 2.9 | 3.4 | 3.7 | 2.6 | 1.8 | 1.8 | | | | 2.4 | 2.2 | 4.1 | 1.8 |
| Dy | 11.4 | 20.2 | 15.0 | 17.6 | 19.2 | 14.9 | 10.1 | 10.4 | | | | 12.3 | 11.7 | 20.9 | 9.4 |
| Ho | | | | | | | 2.0 | 2.1 | | | | 2.5 | 2.3 | 4.2 | 1.9 |
| Er | 5.3 | 9.3 | 6.9 | 8.6 | 9.1 | 8.6 | 5.3 | 5.0 | | | | 5.8 | 5.6 | 10.2 | 4.5 |
| Tm | | | | | | | 0.7 | 0.6 | | | | 0.8 | 0.7 | 1.4 | 0.7 |
| Yb | 4.5 | 8.4 | 5.5 | 6.7 | 7.5 | 6.5 | 4.4 | 3.6 | | | | 4.9 | 4.6 | 8.2 | 3.8 |
| Lu | 0.55 | 1.03 | 0.75 | 0.86 | 1.10 | 0.81 | 0.63 | 0.48 | | | | 0.73 | 0.71 | 1.17 | 0.53 |
| $(La/Yb)_n$ | 15 | 18 | 16 | 15 | 16 | 13 | 17 | 17 | | | | 19 | 19 | 16 | 19 |
| Eu/Eu* | 0.85 | 0.76 | 0.79 | 0.71 | 0.78 | 0.79 | 0.75 | 0.76 | | | | 0.76 | 0.75 | 0.53 | 0.94 |
| MALI | 5.68 | 1.25 | 1.96 | 0.95 | 1.25 | 2.77 | 2.56 | 1.76 | 4.28 | 4.59 | 4.50 | 2.59 | 3.84 | 1.01 | 4.62 |
| Fe* | 0.75 | 0.81 | 0.80 | 0.80 | 0.82 | 0.80 | 0.80 | 0.80 | 0.82 | 0.81 | 0.80 | 0.80 | 0.81 | 0.85 | 0.81 |
| ASI | 0.97 | 0.89 | 0.92 | 0.90 | 0.88 | 0.94 | 0.93 | 0.92 | 0.95 | 0.95 | 0.94 | 0.92 | 0.93 | 0.84 | 0.94 |
| Agp | 0.70 | 0.61 | 0.61 | 0.59 | 0.62 | 0.63 | 0.62 | 0.60 | 0.68 | 0.70 | 0.68 | 0.63 | 0.67 | 0.64 | 0.69 |
| T sat zrn | 898 | 894 | 904 | 899 | 906 | 966 | 867 | 873 | 919 | 914 | 886 | 887 | 910 | 896 | 885 |
| T sat ap | 1012 | 1090 | 1079 | 1034 | 1067 | 1047 | 1003 | 1022 | 1046 | 1045 | 1013 | 1045 | 1045 | 1018 | 1019 |

Fe* = FeOt/(FeOt + MgO); MALI = $Na_2O + K_2O - CaO$ (modified alkali-lime index of Frost *et al.* 2001); ASI = $Al_2O_3/(Na_2O + K_2O + CaO - 3.3P_2O_5)$; Agp = $(Na_2O + K_2O)/Al_2O_3$ (molar proportions). Major elements normalized to 100 wt%. T sat zrn and T sat ap are the temperatures of saturation of zircon and apatite, respectively (Watson & Harrison 1983, Harrison & Watson 1984).

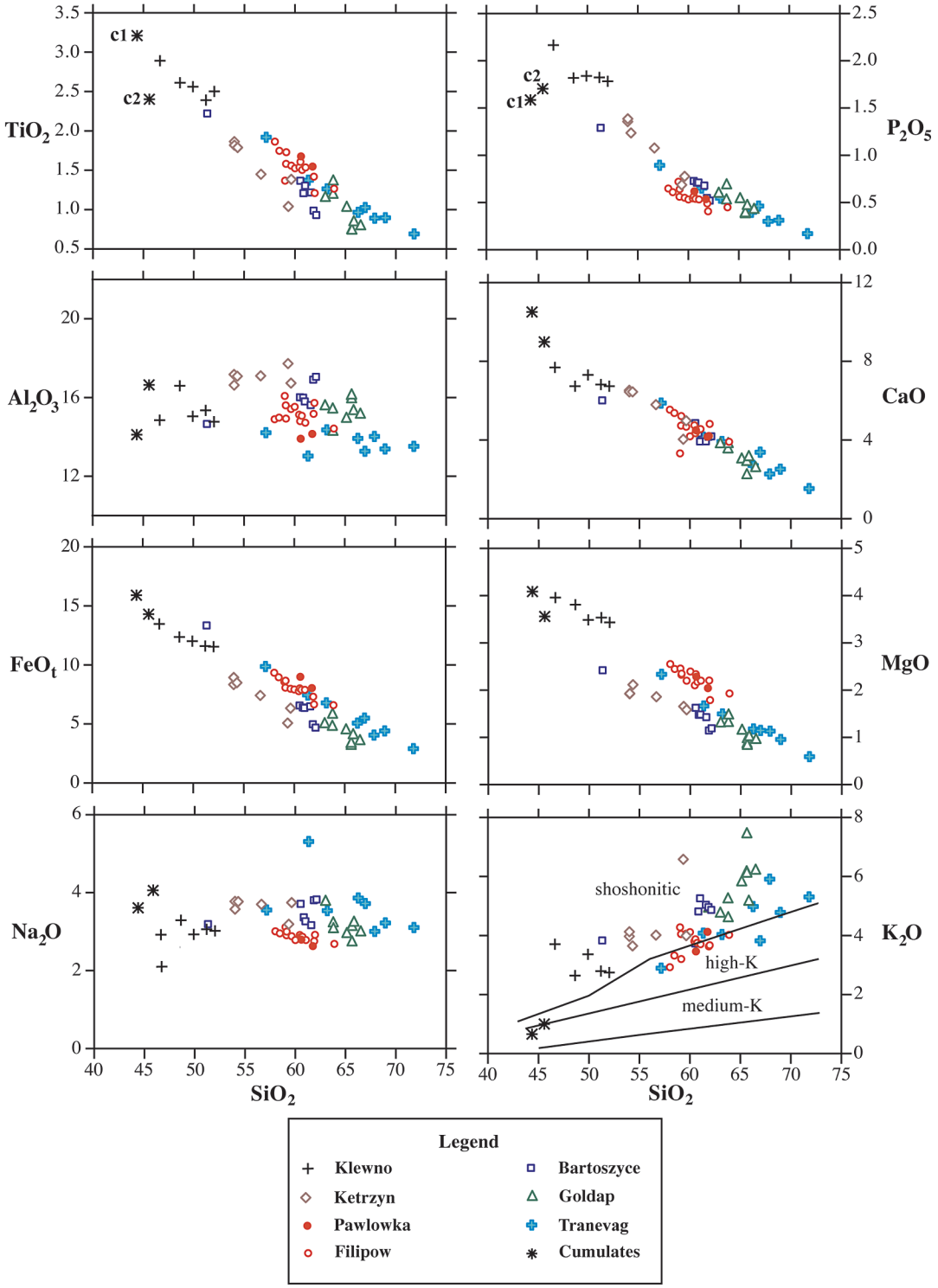
TiO2
P2O5
Al2O3
CaO
FeOt
MgO
Na2O
K2O
SiO2
SiO2
c1
c2
c2
c1
shoshonitic
high-K
medium-K
Legend
Klewno
Ketrzyn
Pawlowka
Filipow
Bartoszyce
Goldap
Tranevag
Cumulates

order to discriminate between these two mechanisms, the contrasting behavior of compatible and incompatible elements can be used. A plot of log (compatible element) *versus* log (incompatible element) allows for the distinction between the two mechanisms, with partial melting resulting in a subhorizontal trend and fractional crystallization giving a subvertical trend (Cocherie 1986, Martin 1987, Martin *et al.* 1994). Figure 9 shows that all samples define a vertical trend typical of fractional crystallization rather than of partial melting. This conclusion is corroborated by the fact that several mineral phases are zoned. Even if zoning always remains of limited extent, it shows that the magma from which these minerals crystallized underwent fractional crystallization. Consequently, the subsequent discussions will focus on a fractional crystallization process.

*Modeling the fractional crystallization process*

Comparison with the South Norway HBG allows to decipher the petrogenesis of the Mazury suite. In South Norway, the compositions of the parental magma and conjugate liquidus minerals have been studied experimentally (Bogaerts *et al.* 2003, 2006) and this approach provides strong constraints on the proposed petrogenetic model. Using mass-balance equations, Bogaerts *et al.* (2003) have calculated the modal compositions of two cumulates $c_1$ and $c_2$ in equilibrium with the liquids at 56 wt% and 62.5 wt% $SiO_2$, respectively, on the Tranevåg liquid line of descent. The calculated compositions of the minerals and their proportions in cumulates $c_1$ and $c_2$ are given in Table 5, together with the whole-rock compositions of the cumulates and their conjugate melts (Fig. 3). These cumulates $c_1$ and $c_2$ can explain the Klewno diorites, which are low-silica rocks ($SiO_2$ <56 wt%) with high P, Ti and Fe contents. These rocks could represent liquids, cumulates or crystal-laden melts. Indeed, for most major elements, the compositions of the Klewno samples plot on linear arrays joining the cumulate composition to the starting composition of the Tranevåg liquid line of descent. It can thus be inferred that the Klewno samples represent a mixture of cumulus minerals and their conjugate melt. The composition of the $c_2$ cumulate plots on the prolongation of the Mazury trend in such a way that it is not possible to determine with major elements whether samples with $SiO_2$ above 56 wt% are melts or crystal-laden melts. The clustering of the Filipów and Pawłówka samples along the general trend and their overall similarities of composition to the Tranevåg primitive melt (Fig. 3), however, suggests that these samples are close to melt compositions. Below, we use trace-element concentrations to show that the Kętrzyn, Bartoszyce and Gołdap samples are also crystal-laden melts with variable amounts of cumulus minerals.

Slight differences, however, exist between the Tranevåg liquid line of descent and the Mazury trend, indicating that the two HBG suites did not crystallize under strictly identical conditions or from the same parent magmas. The most striking difference is in $P_2O_5$, which is higher in the Klewno samples, implying a cumulate somewhat richer in apatite (*ca.* 2.5 wt% $P_2O_5$) than the calculated cumulates at Tranevåg.

*Trace elements confirm fractional crystallization*

From the Ce–$P_2O_5$ relationship in Figure 7, it is possible to estimate the REE contents of the apatite in the Klewno samples and the $Kd^{ap/melt}_{REE}$ values. Accepting that these samples lie on a tie-line between apatite and a melt with 0.5–0.7 wt% $P_2O_5$ and 200–300 ppm Ce (similar to the most primitive Tranevåg melt), then apatite should contain about 1.1 wt% Ce. This high value would imply a $Kd_{Ce}^{ap/melt}$ ranging from 37 to 50, values that are realistic for intermediate melts (Henderson 1982, Rollinson 1993). The relatively small variations in REE concentrations between samples on the main trend, such as Filipów and Gołdap, are explained by the buffering role of apatite in the cumulate, leading to bulk partition-coefficients close to one. For example, based on data presented in Table 5 and the above $Kd_{Ce}^{ap/melt}$ values, the bulk partition-coefficient $D_{REE}$ $\left( D = \sum_{n}^{i=1} Kd_{REE}^{i/melt} Xi \right)$ ranges from 1.5 to 2, thus accounting for the very slight decrease in

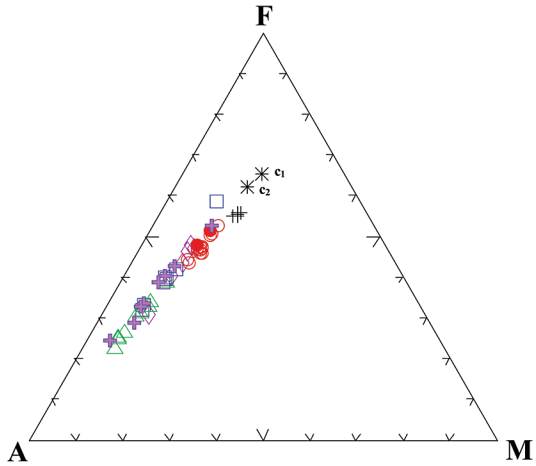


FIG. 3. Major-element compositions of whole rocks plotted in Harker diagrams. In the $K_2O$ *versus* $SiO_2$ diagram, the dividing lines are from Peccerillo & Taylor (1976). The Tranevåg compositions (southern Norway) are from Bogaerts *et al.* (2003), and the cumulate compositions are taken from Table 5.

FIG. 4. A ($Na_2O+K_2O$) – F (FeOt) – M (MgO) diagram. Same legend as in Figure 3.

TABLE 3b. MAJOR- AND TRACE-ELEMENT COMPOSITION OF SAMPLES FROM BOREHOLES IN THE MAZURY COMPLEX

| | Filipow | | | | | | | | | | | | | |
|---|---|---|---|---|---|---|---|---|---|---|---|---|---|---|
| | F1 | F2 | F3 | F4 | F5 | F6 | F7 | F8 | F9 | F10 | F11 | F13 | F14 | F15 |
| $SiO_2$ wt% | 60.01 | 61.88 | 59.02 | 63.88 | 60.71 | 60.45 | 59.12 | 59.64 | 61.05 | 60.55 | 59.14 | 58.01 | 58.46 | 61.96 |
| $TiO_2$ | 1.52 | 1.42 | 1.37 | 1.27 | 1.50 | 1.54 | 1.58 | 1.56 | 1.54 | 1.61 | 1.73 | 1.86 | 1.75 | 1.21 |
| $Al_2O_3$ | 15.52 | 15.17 | 16.08 | 14.42 | 15.07 | 15.13 | 15.60 | 15.42 | 14.72 | 14.80 | 14.93 | 14.90 | 14.98 | 15.72 |
| $Fe_2O_3t$ | 8.80 | 8.11 | 9.51 | 7.32 | 8.78 | 8.64 | 8.96 | 8.87 | 8.76 | 8.90 | 9.62 | 10.38 | 9.94 | 7.39 |
| MnO | 0.13 | 0.13 | 0.12 | 0.11 | 0.13 | 0.13 | 0.15 | 0.15 | 0.14 | 0.15 | 0.16 | 0.17 | 0.16 | 0.11 |
| MgO | 2.39 | 2.20 | 2.46 | 1.93 | 2.17 | 2.10 | 2.32 | 2.20 | 2.20 | 2.34 | 2.35 | 2.55 | 2.45 | 1.79 |
| CaO | 4.19 | 4.20 | 3.32 | 3.91 | 4.47 | 4.75 | 4.73 | 4.67 | 4.55 | 4.35 | 5.22 | 5.54 | 5.37 | 4.82 |
| $Na_2O$ | 2.78 | 2.75 | 3.12 | 2.68 | 2.87 | 2.91 | 2.91 | 2.88 | 2.78 | 2.86 | 3.00 | 3.01 | 2.95 | 2.92 |
| $K_2O$ | 4.11 | 3.63 | 4.28 | 4.02 | 3.75 | 3.80 | 4.05 | 4.06 | 3.71 | 3.87 | 3.20 | 2.93 | 3.32 | 3.67 |
| $P_2O_5$ | 0.53 | 0.49 | 0.72 | 0.45 | 0.53 | 0.54 | 0.56 | 0.55 | 0.53 | 0.57 | 0.64 | 0.65 | 0.61 | 0.41 |
| Th ppm | 9 | 8 | 9 | 10 | 13 | 11 | 11 | 9 | 16 | 14 | 16 | 17 | 20 | 11 |
| Zr | 497 | 454 | 327 | 410 | 500 | 486 | 497 | 444 | 478 | 494 | 510 | 525 | 500 | 365 |
| Nb | 19 | 23 | 24 | 17 | 17 | 18 | 20 | 19 | 19 | 20 | 21 | 22 | 22 | 15 |
| Rb | 177 | 149 | 207 | 127 | 121 | 120 | 122 | 114 | 124 | 130 | 114 | 108 | 123 | 119 |
| Sr | 356 | 346 | 255 | 343 | 359 | 368 | 383 | 369 | 347 | 354 | 352 | 367 | 358 | 383 |
| Ba | 1968 | 1925 | 1254 | 1926 | 1795 | 1875 | 2099 | 2121 | 1740 | 1858 | 1434 | 1560 | 1630 | 1885 |
| V | 138 | 134 | 130 | 121 | 142 | 138 | 153 | 147 | 141 | 147 | 154 | 164 | 159 | 115 |
| Zn | 149 | 128 | 120 | 123 | 139 | 136 | 146 | 142 | 144 | 165 | 155 | 169 | 161 | 119 |
| Co | 23 | 19 | 22 | 12 | 18 | 19 | 23 | 21 | 17 | 21 | 21 | 20 | 23 | 16 |
| Cu | 29 | 39 | 30 | 18 | 28 | 22 | 25 | 23 | 29 | 28 | 28 | 30 | 31 | 18 |
| Pb | 12 | 20 | 21 | 25 | 25 | 24 | 28 | 27 | 24 | 29 | 23 | 22 | 24 | 28 |
| Y | 37 | 52 | 103 | 40 | 45 | 45 | 47 | 47 | 45 | 50 | 56 | 56 | 54 | 37 |
| La | 56 | | | | 94 | | | 89 | | | | 101 | | |
| Ce | 125 | | | | 188 | | | 178 | | | | 206 | | |
| Pr | 16 | | | | 22 | | | 21 | | | | 24 | | |
| Nd | 71 | | | | 86 | | | 83 | | | | 96 | | |
| Sm | 12 | | | | 15 | | | 15 | | | | 17 | | |
| Eu | 3.5 | | | | 3.7 | | | 3.7 | | | | 3.8 | | |
| Gd | 10.0 | | | | 11.4 | | | 11.4 | | | | 13.3 | | |
| Tb | 1.4 | | | | 1.5 | | | 1.6 | | | | 1.8 | | |
| Dy | 7.8 | | | | 8.7 | | | 8.8 | | | | 10.5 | | |
| Ho | 1.5 | | | | 1.7 | | | 1.8 | | | | 2.1 | | |
| Er | 3.7 | | | | 4.5 | | | 4.6 | | | | 5.4 | | |
| Tm | 0.5 | | | | 0.6 | | | 0.6 | | | | 0.7 | | |
| Yb | 3.0 | | | | 3.6 | | | 3.5 | | | | 4.4 | | |
| Lu | 0.44 | | | | 0.47 | | | 0.50 | | | | 0.64 | | |
| $(La/Yb)_n$ | 12 | | | | 17 | | | 16 | | | | 15 | | |
| Eu/Eu* | 0.96 | | | | 0.88 | | | 0.89 | | | | 0.79 | | |
| MALI | 2.65 | 2.14 | 3.96 | 2.74 | 2.11 | 1.92 | 2.18 | 2.23 | 1.89 | 2.32 | 0.97 | 0.39 | 0.89 | 1.74 |
| Fe* | 0.77 | 0.77 | 0.78 | 0.77 | 0.78 | 0.79 | 0.78 | 0.78 | 0.78 | 0.77 | 0.79 | 0.79 | 0.79 | 0.79 |
| ASI | 1.00 | 1.01 | 1.13 | 0.97 | 0.96 | 0.92 | 0.94 | 0.94 | 0.94 | 0.95 | 0.91 | 0.89 | 0.89 | 0.94 |
| Agp | 0.58 | 0.56 | 0.61 | 0.61 | 0.58 | 0.59 | 0.59 | 0.59 | 0.58 | 0.60 | 0.56 | 0.54 | 0.56 | 0.56 |
| T sat zrn | 873 | 870 | 845 | 859 | 869 | 860 | 861 | 851 | 861 | 866 | 855 | 851 | 848 | 841 |
| T sat ap | 971 | 985 | 999 | 995 | 986 | 978 | 970 | 975 | 984 | 980 | 992 | 984 | 977 | 962 |

Fe* = FeOt/(FeOt + MgO); MALI = $Na_2O + K_2O - CaO$ (modified alkali-lime index of Frost *et al.* 2001); ASI = $Al_2O_3/(Na_2O + K_2O + CaO - 3.3P_2O_5)$; Agp = $(Na_2O + K_2O)/Al_2O_3$ (molar proportions). Major elements normalized to 100 wt%. T sat zrn and T sat ap are the temperatures of saturation of zircon and apatite, respectively (Watson & Harrison 1983, Harrison & Watson 1984).

the REE content during fractionation, and also for the subparallel character of the REE patterns among the various samples (Fig. 8). The Kętrzyn, Bartoszyce and Gołdap samples, which roughly plot on linear arrays in a Ce–$SiO_2$ diagram (Fig. 5g), appear to be mixtures of cumulus minerals and melts that could be represented by the most evolved sample of the series, *i.e.*, samples containing *ca*. 59, 61 and 67 wt% $SiO_2$, respectively.

The small variation in whole-rock Sr concentrations observed within each intrusion (Fig. 5) can also be explained with a bulk partition-coefficient $D_{Sr}$ close to 1. Given that $Kd_{Sr}^{pl/melt} = 2$ in melts of intermediate compositions, whereas $Kd_{Sr}^{i/melt} << 1$ in all other cumulative minerals *i* (*e.g.*, Rollinson 1993), and that cumulates in these melts contain about 50% plagioclase (see $c_1$ and $c_2$ in Table 5), the bulk partition-coefficient

TABLE 3c. MAJOR- AND TRACE-ELEMENT COMPOSITION OF SAMPLES FROM BOREHOLES IN THE MAZURY COMPLEX

| | Goldap | | | | | | | | | Klewno | | | | |
|---|---|---|---|---|---|---|---|---|---|---|---|---|---|---|
| | G1 | G1b | G2 | G3 | G4 | G5 | G6 | G7 | G8 | KW1 | KW2 | KW3 | KW4 | KW5 |
| $SiO_2$ wt% | 65.64 | 65.62 | 65.65 | 63.79 | 63.77 | 65.84 | 66.51 | 65.13 | 63.01 | 52.02 | 46.64 | 48.62 | 49.90 | 51.19 |
| $TiO_2$ | 0.75 | 0.76 | 0.75 | 1.38 | 1.21 | 0.86 | 0.81 | 1.04 | 1.17 | 2.50 | 2.89 | 2.61 | 2.56 | 2.39 |
| $Al_2O_3$ | 16.19 | 16.15 | 15.99 | 14.33 | 15.47 | 15.39 | 15.20 | 15.00 | 15.63 | 14.77 | 14.85 | 16.60 | 15.04 | 15.35 |
| $Fe_2O_3t$ | 3.84 | 3.82 | 3.64 | 6.57 | 5.44 | 4.65 | 4.09 | 5.10 | 5.67 | 12.82 | 14.97 | 13.74 | 13.33 | 12.87 |
| MnO | 0.05 | 0.05 | 0.06 | 0.12 | 0.11 | 0.08 | 0.06 | 0.09 | 0.11 | 0.17 | 0.22 | 0.13 | 0.22 | 0.16 |
| MgO | 0.85 | 0.89 | 0.99 | 1.50 | 1.34 | 1.04 | 0.98 | 1.17 | 1.33 | 3.43 | 3.96 | 3.81 | 3.49 | 3.54 |
| CaO | 2.97 | 2.96 | 2.29 | 3.87 | 3.60 | 3.21 | 2.65 | 3.09 | 3.86 | 6.73 | 7.69 | 6.73 | 7.31 | 6.82 |
| $Na_2O$ | 3.16 | 3.16 | 2.76 | 3.10 | 3.25 | 3.27 | 3.02 | 2.98 | 3.80 | 3.02 | 2.92 | 3.29 | 2.93 | 3.06 |
| $K_2O$ | 6.15 | 6.19 | 7.48 | 4.64 | 5.28 | 5.20 | 6.25 | 5.85 | 4.79 | 2.74 | 3.71 | 2.64 | 3.36 | 2.80 |
| $P_2O_5$ | 0.40 | 0.40 | 0.39 | 0.70 | 0.54 | 0.48 | 0.44 | 0.55 | 0.61 | 1.78 | 2.17 | 1.82 | 1.84 | 1.82 |
| Th ppm | | | 15 | 25 | 22 | 15 | 14 | 19 | | 4 | 6 | 6 | 6 | 5 |
| Zr | 411 | 419 | 336 | 671 | 578 | 457 | 439 | 578 | 650 | 639 | 462 | 1171 | 620 | 581 |
| Nb | 15 | 15 | 11 | 33 | 31 | 15 | 20 | 26 | 29 | 41 | 45 | 33 | 37 | 30 |
| Rb | 192 | 191 | 233 | 170 | 180 | 173 | 205 | 196 | 167 | 69 | 82 | 94 | 86 | 73 |
| Sr | 398 | 390 | 383 | 320 | 351 | 348 | 359 | 353 | 351 | 858 | 745 | 712 | 831 | 822 |
| Ba | 1992 | 1941 | 2344 | 1394 | 1701 | 1606 | 1883 | 1874 | 1516 | 2433 | 2110 | 1567 | 2487 | 2135 |
| V | 44 | 50 | 37 | 93 | 61 | 47 | 50 | 57 | 69 | 238 | 244 | 254 | 257 | 238 |
| Zn | 39 | 42 | 74 | 130 | 111 | 93 | 74 | 96 | 129 | 218 | 299 | 256 | 270 | 215 |
| Co | 8 | 6 | 6 | 7 | 3 | 3 | 5 | 5 | 8 | 30 | 33 | 27 | 28 | 22 |
| Cu | 10 | 10 | 10 | 10 | 10 | 10 | 10 | 10 | 10 | 51 | 68 | 27 | 67 | 41 |
| Ga | 22 | 23 | 21 | 24 | 23 | 22 | 22 | 22 | 24 | 24 | 27 | 30 | 26 | 27 |
| Pb | 37 | 34 | 39 | 34 | 33 | 36 | 35 | 36 | 34 | 24 | 19 | 20 | 26 | 22 |
| Y | 43 | 41 | 38 | 97 | 76 | 44 | 33 | 56 | 68 | 78 | 102 | 76 | 80 | 69 |
| La | | | 105 | 163 | 153 | 116 | 114 | 144 | | | 265 | 243 | | |
| Ce | | | 225 | 390 | 336 | 238 | 234 | 301 | | | 574 | 517 | | |
| Pr | | | 25 | 45 | 41 | 28 | 27 | 36 | | | 69 | 61 | | |
| Nd | | | 99 | 174 | 141 | 102 | 101 | 130 | | | 282 | 238 | | |
| Sm | | | 17 | 31 | 28 | 18 | 17 | 23 | | | 46 | 37 | | |
| Eu | | | 3.1 | 5.2 | 5.4 | 3.3 | 2.8 | 4.0 | | | 8.1 | 7.0 | | |
| Gd | | | 11.8 | 21.2 | 20.2 | 12.1 | 10.4 | 14.1 | | | 31.1 | 25.3 | | |
| Tb | | | 1.9 | 3.0 | 2.9 | 1.9 | 1.5 | 2.1 | | | 4.0 | 3.1 | | |
| Dy | | | 10.3 | 18.5 | 16.8 | 10.8 | 8.5 | 12.4 | | | 20.9 | 16.0 | | |
| Ho | | | 2.2 | 3.9 | 3.5 | 2.3 | 1.9 | 2.6 | | | 3.8 | 3.0 | | |
| Er | | | 5.6 | 9.9 | 9.1 | 5.8 | 4.7 | 6.7 | | | 9.4 | 7.3 | | |
| Tm | | | 0.8 | 1.5 | 1.3 | 0.8 | 0.7 | 1.0 | | | 1.2 | 0.9 | | |
| Yb | | | 5.0 | 9.4 | 8.5 | 5.7 | 4.6 | 6.7 | | | 6.9 | 5.2 | | |
| Lu | | | 0.76 | 1.55 | 1.31 | 0.83 | 0.72 | 1.07 | | | 0.95 | 0.71 | | |
| $(La/Yb)_n$ | | | 13 | 11 | 12 | 13 | 16 | 14 | | | 25 | 30 | | |
| Eu/Eu* | | | 0.68 | 0.62 | 0.70 | 0.68 | 0.64 | 0.69 | | | 0.66 | 0.70 | | |
| MALI | 6.32 | 6.41 | 7.92 | 3.88 | 4.94 | 5.26 | 6.64 | 5.73 | 4.74 | -0.96 | -1.05 | -0.79 | -1.00 | -0.95 |
| Fe* | 0.80 | 0.79 | 0.77 | 0.80 | 0.79 | 0.80 | 0.79 | 0.80 | 0.79 | 0.77 | 0.77 | 0.76 | 0.78 | 0.77 |
| ASI | 0.98 | 0.98 | 0.99 | 0.92 | 0.94 | 0.97 | 0.97 | 0.95 | 0.91 | 0.92 | 0.84 | 1.02 | 0.86 | 0.95 |
| Agp | 0.73 | 0.74 | 0.79 | 0.71 | 0.71 | 0.71 | 0.77 | 0.75 | 0.73 | 0.54 | 0.59 | 0.50 | 0.56 | 0.53 |
| T sat zrn | 872 | 873 | 854 | 900 | 893 | 880 | 878 | 898 | 900 | 826 | 748 | 895 | 802 | 819 |
| T sat ap | 1013 | 1017 | 1009 | 1077 | 1039 | 1042 | 1041 | 1051 | 1047 | 1081 | 1043 | 1029 | 1052 | 1073 |

Fe* = FeOt/(FeOt + MgO); MALI = $Na_2O + K_2O - CaO$ (modified alkali-lime index of Frost *et al.* 2001); ASI = $Al_2O_3/(Na_2O + K_2O + CaO - 3.3P_2O_5)$; Agp = $(Na_2O + K_2O)/Al_2O_3$ (molar proportions). Major elements normalized to 100 wt%. T sat zrn and T sat ap are the temperatures of saturation of zircon and apatite, respectively (Watson & Harrison 1983, Harrison & Watson 1984).

$D_{Sr}$ must be close to 1. Consequently, the cumulates, the melts and any mixture of these two components have similar Sr contents.

In the Kętrzyn, Bartoszyce and Gołdap samples, the inverse correlation of Zr with $SiO_2$ (Fig. 5) can be accounted for by the presence of zircon in the cumulate. The temperature of saturation of zircon (Watson & Harrison 1983) is in the range 800–920°C range (Table 3), in agreement with the high liquidus temperature of ferroan granites (*e.g.,* Duchesne & Wilmart 1997, Dall'Agnol *et al*. 1999, Bogaerts *et al*. 2006). In the Klewno samples, Zr concentrations are low (except in one sample), which suggests that zircon is not an accumulated phase, but crystallized from the melt component in these crystal-laden samples.

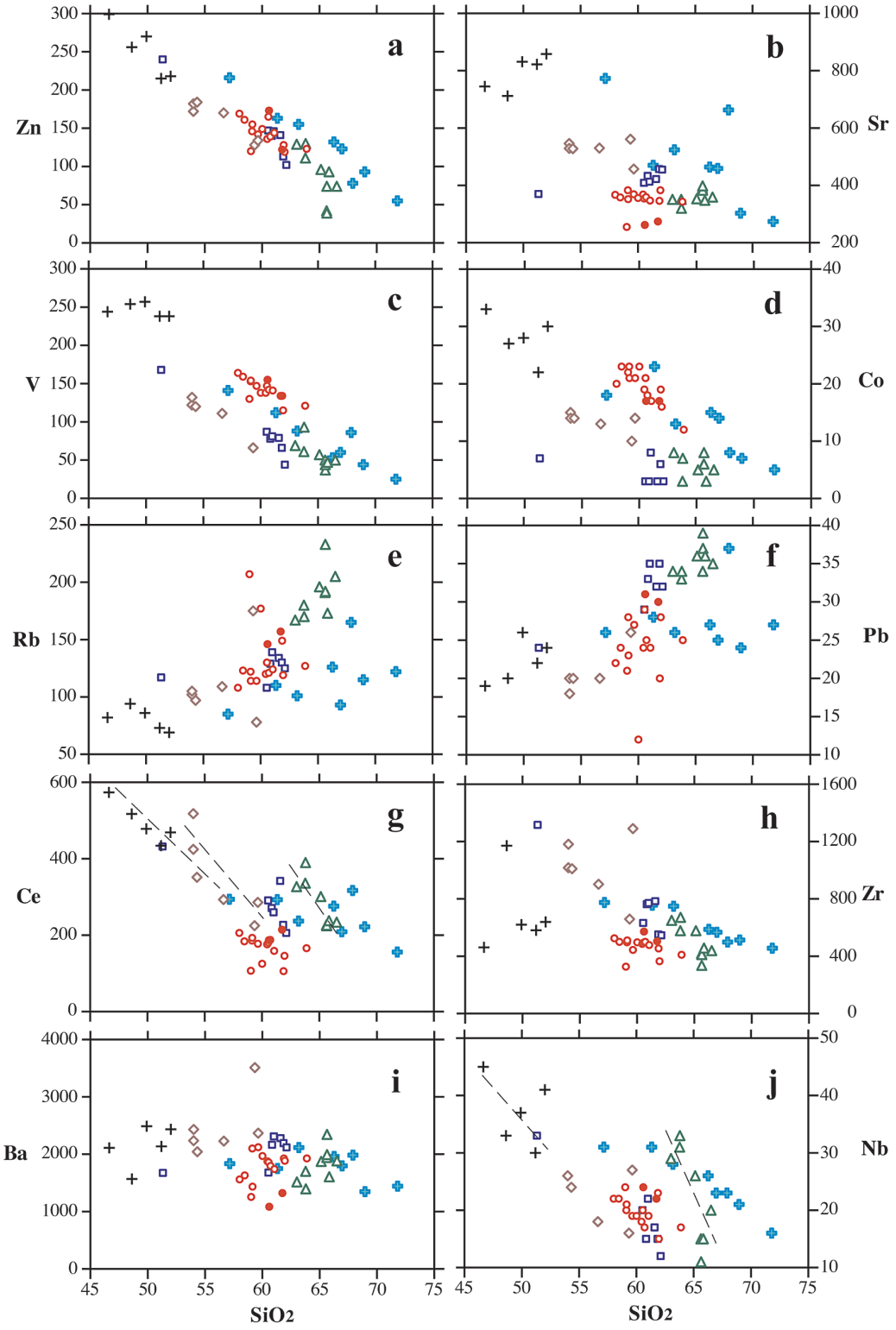
a
b
c
d
e
f
g
h
i
j
Zn
Sr
V
Co
Rb
Pb
Ce
Zr
Ba
Nb
SiO2
SiO2

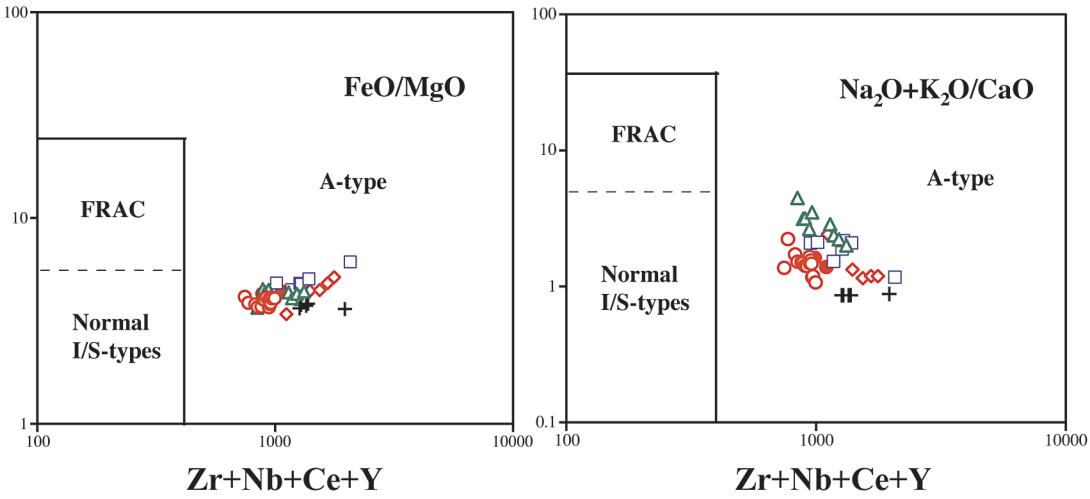


FIG. 6. FeOt/MgO and $(Na_2O + K_2O)/CaO$ *versus* Zr+Nb+Ce+Y diagrams, after Whalen *et al.* (1987). Same legend as in Figure 3. FRAC defines the field of fractionated I- and S- types granites.

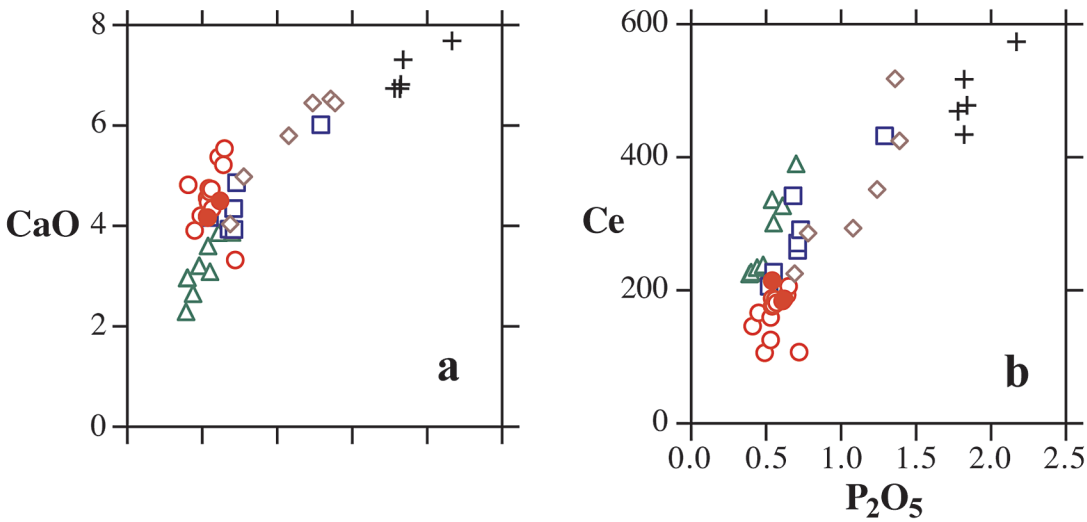


FIG. 7. a. Whole-rock CaO *versus* $P_2O_5$ ; b. Whole-rock Ce *versus* $P_2O_5$ contents. Same symbols as in Figure 3.

FIG. 5. Trace-element concentrations plotted in Harker diagrams. Same legend as in Figure 3. The dashed lines outline possible trends in some intrusions.

Another line of evidence in favor of fractional crystallization is provided by linear arrays in log–log coordinates (Fig. 9). The slope of the Zn and V evolutions allows for an evaluation of $D_{Zn}$ and $D_V$, assuming $D_{Rb} < 0.1$ (incompatible behavior). The calculated $D_{Zn}$ and $D_V$ ranges between 3 and 4. Given that magnetite, the main Zn- and V-bearing phase, is present in the $c_1$ and $c_2$ cumulates with a fraction of 11wt% (Table 5), this yields $Kd_{Zn}^{mgt/melt}$ and $Kd_V^{mgt/melt}$ ranging from 27

to 36, values that are realistic for melts of intermediate compositions (*e.g.*, Ewart & Griffin 1994).

In summary, the overall trend observed in all geochemical diagrams for the Mazury intrusions is defined by a series of magma batches, each one referring to a specific pluton and having undergone limited amounts of fractionation. The samples from an intrusion do not generally correspond to pure melts, but rather to melts laden with variable amounts of cumulus minerals. Thus, the overall trend cannot properly represent a liquid line of descent, but a collection of pure melts mixed with melts more or less loaded with cumulus minerals. With our model, however, we have identified true melts at 56, 59, 61 and 67 wt% $SiO_2$, which are linked by a fractional crystallization process. In detail some of the magma batches appear to have slightly different trace-element signatures (Fig. 4), which very likely result from small variations in source composition or conditions of partial melting.

*Constraints on source age and composition*

The isotopic data (Table 4) give insights into the timing and nature of the source rocks of the various magmas. In a diagram of an $\varepsilon_{Nd(T)}$ *versus* $(^{87}Sr/^{86}Sr)_0$ (Fig. 10), all samples plot far from the mantle array, which is consistent with crustal input in the source of the Mazury magmas. The source of the granites could be either older continental crust, or a mixture of mantle material and older continental crust. In the latter case, the crustal component should be significantly older than the observed model ages, very probably of Archean age. However, all available results on the Precambrian basement of the East European Craton (Claesson *et al.* 2001), and particularly on its Polish part (Claesson & Ryka 1999), preclude the existence of Archean material in that region. This constitutes a compelling argument in favor of a Paleoproterozoic continental crustal source for the Mazury magmas.

There is no linear relationship between $^{87}Sr/^{86}Sr$ and 1/Sr (Fig. 11a) in support of a mixing process, and, if $\varepsilon_{Nd}$ or $(^{87}Sr/^{86}Sr)_0$ are plotted *versus* $SiO_2$ (Figs. 11b, c), there is no correlation between isotopic values and silica content, which suggests a limited role for assimilation – fractional crystallization (AFC). In particular, the two Bartoszyce samples B4 and B6 show similar isotopic values, around 0.704, for quite different $SiO_2$ contents (Table 4).

The samples from the Kętrzyn, Bartoszyce, Filipów and Gołdap massifs give very similar $T_{DM}$ ages of ~2.18 Ga (Table 4, Fig. 12). Their parental magmas could thus have been derived from the melting of a single protolith extracted from a depleted mantle at about 2.18 Ga, assuming that the latter had an average $^{147}Sm/^{144}Nd$ of 0.1071. The Klewno sample shows a somewhat younger $T_{DM}$ (2.04 Ga), which could be explained either by melting a protolith extracted from the mantle 140 million years after the extraction of the protolith of other massifs, or by a two stage-evolution. In this latter scenario, the extraction of the protolith from the mantle took place at about 2.18 Ga but, in contast to the samples from the other intrusions, it evolved with a $^{147}Sm/^{144}Nd$ equal to 0.1257 (Fig. 12). At 1.5 Ga, melting and differentiation of the protolith changed the $^{147}Sm/^{144}Nd$ into the measured one (0.0976). However, as the differentiation of the Klewno melts implies subtraction of a cumulate with more than 3% apatite (Table 5), the REE budget would have been completely controlled by this phase. As $Kd^{ap/melt}_{Nd} < Kd^{ap/melt}_{Sm}$ (Watson & Green 1981, Henderson 1982, Rollinson 1993), the Sm/Nd value of the Klewno cumulate would be higher than that of the liquid from which it is extracted, whatever the proportion of trapped liquid in the cumulate. This is inconsistent with the measured Sm/Nd (0.0976); therefore, the hypothesis must be rejected. For the sample from the Pawłówka drillcore, we suggest that the lower $\varepsilon_{Nd}$ value relative to the other intrusions can reflect a possible contamination at the age

TABLE 4. Rb–Sr AND Sm–Nd ISOTOPIC COMPOSITIONS OF SELECTED SAMPLES FROM BOREHOLES IN THE MAZURY COMPLEX

| | $SiO_2$ % | Rb ppm | Sr ppm | $^{87}Rb/^{86}Sr$ | $^{87}Sr/^{86}Sr$ | ± 2σ | $(^{87}Sr/^{86}Sr)$ 1500 Ma | Sm ppm | Nd ppm | $^{147}Sm/^{144}Nd$ | $^{143}Nd/^{144}Nd$ | ± 2σ | $(^{143}Nd/^{144}Nd)$ 1500 Ma | $(\varepsilon_{Nd})_t$ | $T_{DM}$ Ma |
|---|---|---|---|---|---|---|---|---|---|---|---|---|---|---|---|
| Kw 2 | 46.30 | 82 | 745 | 0.319 | 0.710496 | 0.000009 | 0.70364 | 45.6 | 282.5 | 0.0976 | 0.511492 | 0.000010 | 0.51053 | -3.3 | 2036 |
| K 5 | 57.86 | 109 | 530 | 0.596 | 0.717335 | 0.000009 | 0.70451 | 25.1 | 143.7 | 0.1057 | 0.511515 | 0.000010 | 0.51047 | -4.4 | 2158 |
| P 144 | 60.75 | 146 | 262 | 1.618 | 0.741254 | 0.000009 | 0.70642 | 16.1 | 84.0 | 0.1159 | 0.511493 | 0.000010 | 0.51035 | -6.8 | 2424 |
| F 13 | 59.74 | 108 | 367 | 0.853 | 0.724976 | 0.000009 | 0.70661 | 16.7 | 96.2 | 0.1047 | 0.511499 | 0.000010 | 0.51047 | -4.6 | 2162 |
| B 6 | 51.29 | 117 | 370 | 0.916 | 0.723441 | 0.000009 | 0.70371 | 40.5 | 219.0 | 0.1118 | 0.511552 | 0.000010 | 0.51045 | -4.9 | 2234 |
| B 4 | 60.66 | 108 | 409 | 0.765 | 0.720319 | 0.000009 | 0.70385 | 23.8 | 137.0 | 0.1050 | 0.511507 | 0.000010 | 0.51047 | -4.5 | 2157 |
| G 3 | 63.96 | 170 | 320 | 1.541 | 0.735106 | 0.000009 | 0.70192 | 31.1 | 174.0 | 0.1081 | 0.511525 | 0.000010 | 0.51046 | -4.7 | 2193 |

Values of $\varepsilon_{Nd}$ are calculated relative to CHUR with the present $^{143}Nd/^{144}Nd = 0.512638$ (Goldstein *et al.* 1984) and $^{147}Sm/^{143}Nd = 0.1967$ (Jacobsen & Wasserburg 1980). $T_{DM}$ (depleted mantle model ages) are calculated following the parameters of Nelson & DePaolo (1985).

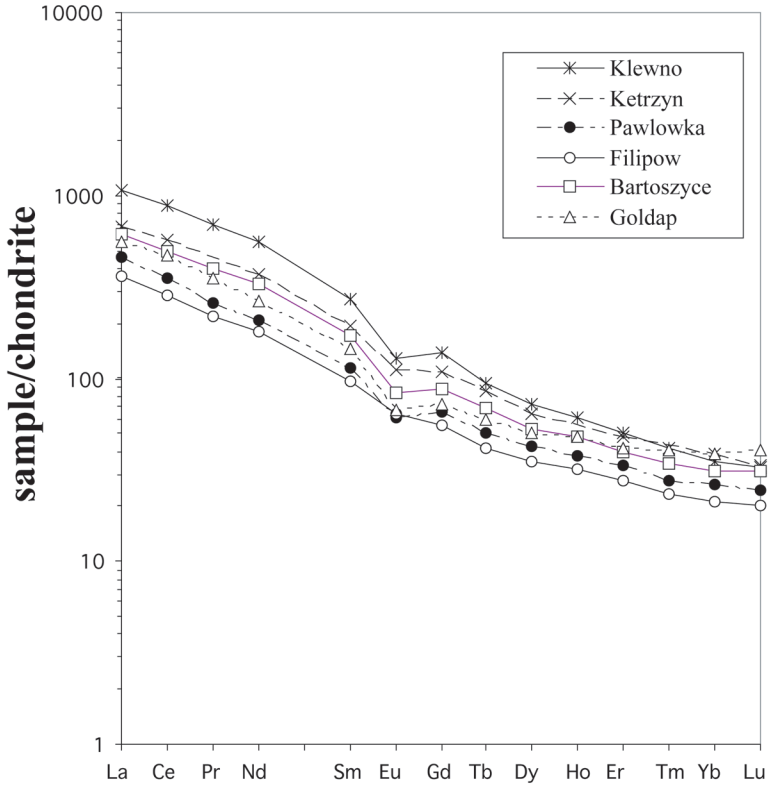


FIG. 8. Chondrite-normalized REE distribution (normalizing values after Sun & McDonough 1989), showing average values for the various groups. Same symbols as in Figure 3.

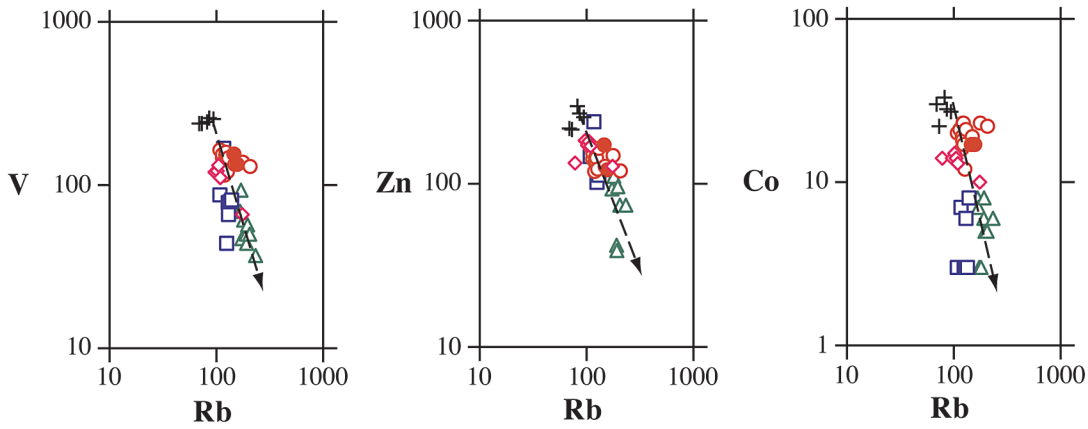


FIG. 9. Log of V, Zn and Co concentrations (compatible elements) *versus* log of Rb concentrations (incompatible element). Same symbols as in Figure 3. The arrows suggest an overall fractional crystallization process.

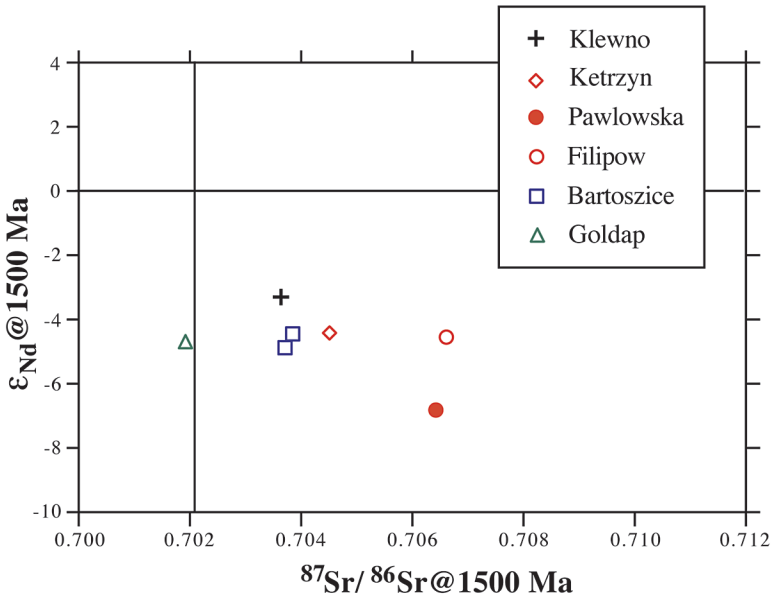


FIG. 10. Values of $\varepsilon_{Nd}$ at1500 Ma *versus* $^{87}Sr/^{86}Sr$ at1500 Ma for seven samples of the Mazury massif.

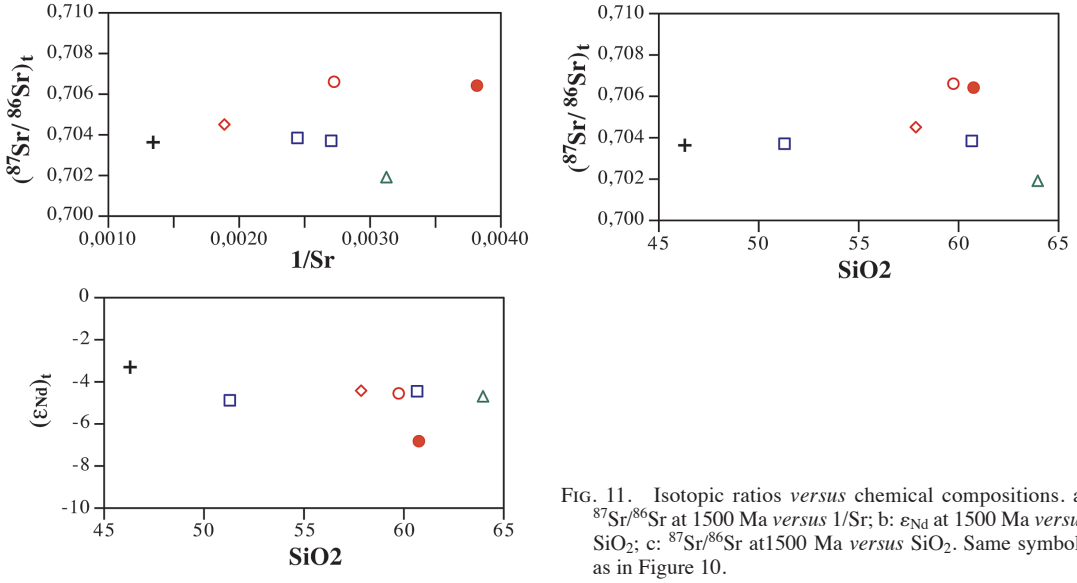


FIG. 11. Isotopic ratios *versus* chemical compositions. a: $^{87}Sr/^{86}Sr$ at 1500 Ma *versus* 1/Sr; b: $\varepsilon_{Nd}$ at 1500 Ma *versus* $SiO_2$; c: $^{87}Sr/^{86}Sr$ at1500 Ma *versus* $SiO_2$. Same symbols as in Figure 10.

of intrusion with a slightly older crustal material (Fig. 12). Finally, the 1.5 Ga anorthosite and ferrodiorite from the Suwalki massif show a range in $\varepsilon_{Nd(T)}$ (–2.5 to –5.3) (Wiszniewska *et al.* 2002) and average $T_{DM}$ (~2.09 Ga) similar to that determined for granitoids from the Kętrzyn, Bartoszyce, Filipów and Gołdap drillcores. Thus we propose that the protoliths of the Mazury HBG suite and of the anorthosite and ferrodiorite were extracted from the mantle at the same time.

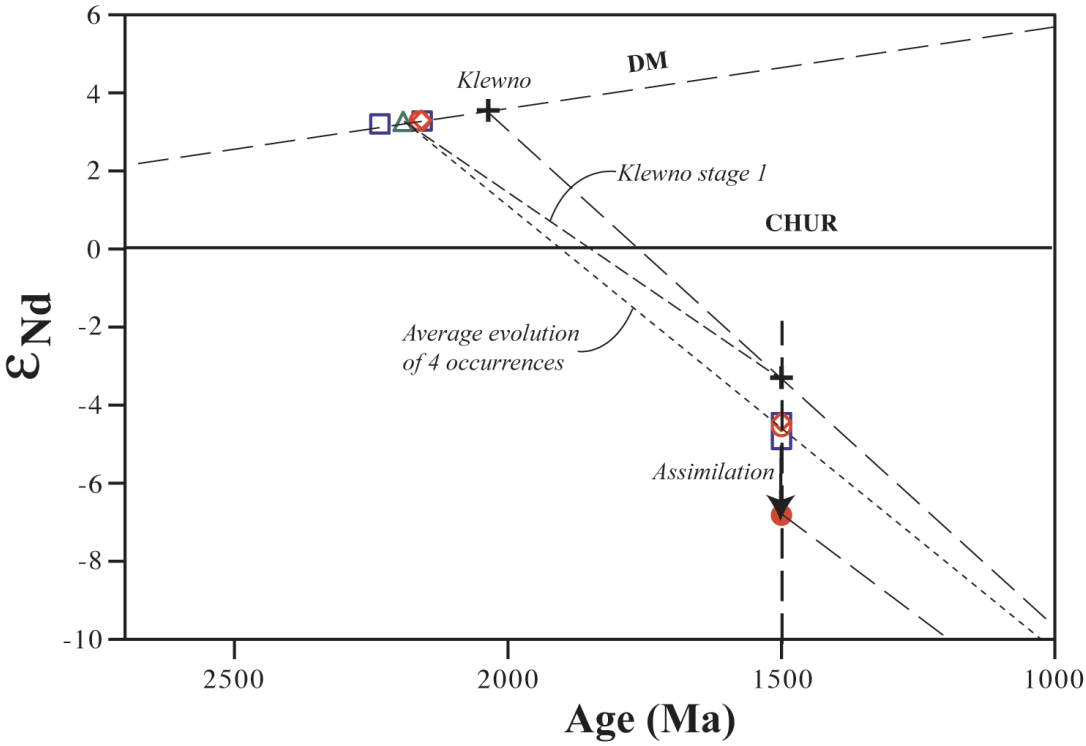


FIG. 12. Values of $\varepsilon_{Nd}$ *versus* age for samples of the Mazury Complex. The age of crystallization of all samples from the Mazury complex is assumed to be 1.5 Ga. The evolution curve of the depleted mantle is after DePaolo (1983). The symbols are the same as in Figure 10. The average evolution of samples from Kętrzyn, Bartoszyce, Filipów, and Gołdap is shown, as well as the hypothetical stage 1 of Klewno (see text for details). For the Pawłówka sample, contamination at the age of intrusion is indicated by the arrow.

The HBG series formed from oxidized melts with a high $H_2O$ content (*e.g.*, Dall'Agnol *et al.* 1999, Bogaerts *et al.* 2006) and anorthosite–ferrodiorite crystallized from dry magmas under reduced conditions (*e.g.*, Frost & Frost 1997, Vander Auwera *et al.* 1998b, 2008). The coexistence in space and time of the two series is intriguing. Longhi *et al.* (1999) have interpreted the parental magma of anorthosite as resulting from the melting of a dry granulitic mafic source, and Vander Auwera *et al.* (2008) have proposed that the HBG series was formed from a mildly hydrous amphibolitic mafic source. Two crustal mafic sources thus differing in $H_2O$ contents appear to have been involved in the Mazury complex, as is also the case in South Norway (Vander Auwera *et al.* 2003).

*Structural setting*

The AMCG Mazury Complex is of batholithic size (350 × 50 km) and was emplaced along a linear structure. Further north, the Nemunas and Geluva intrusions in Lithuania also were emplaced along an east–west lineament (Skridlaite *et al.* 2007). A similar structural setting has also been recognized in several other Proterozoic AMCG complexes, *e.g.*, in the Nain Province (Emslie *et al.* 1994), in the Laramie anorthosite complex (Scoates & Chamberlain 1997), in southern Norway (Duchesne *et al.* 1999, Vander Auwera *et al.* 2003), and in Namaqualand (Duchesne *et al.* 2007). The Madagascar anorthosites are associated with a mega-shear zone (de Wit *et al.* 2001) and the Korosten Complex (Ukraine) has intruded at the intersection of two large lineaments (Bogdanova *et al.* 2004). These structural settings constitute zones of weakness of lithospheric size that likely controlled and favored the emplacement of these large igneous complexes. Linear delamination of the lithosphere along these structures can bring the asthenosphere into contact with the base of the crust, thus providing the additional heat necessary for melting of the lower crust (Teyssier & Tikoff 1998).

TABLE 5. MASS-BALANCE CALCULATION FOR MAJOR ELEMENTS[§]

| | minerals | | | | | | | cumulates | | liquids | | |
|---|---|---|---|---|---|---|---|---|---|---|---|---|
| | Cpx | Hbl (*) | Pl (*) | Mgt (*) | Ilm (*) | Ap | Bt | c1 | c2 | VDA 9925 | VDA 9926 | VDA 9927 |
| $SiO_2$ wt% | 51.88 | 41.82 | 60.16 | 0 | 0 | 0 | 36.62 | 44.16 | 45.15 | 56.34 | 62.50 | 71.69 |
| $TiO_2$ | 0.17 | 2.14 | 0 | 12.1 | 45.12 | 0 | 3.71 | 3.20 | 2.38 | 1.89 | 1.25 | 0.69 |
| $Al_2O_3$ | 1.24 | 10.98 | 23.71 | 2.25 | 0.32 | 0 | 14 | 14.04 | 16.48 | 14.01 | 14.19 | 13.45 |
| FeO | 12.29 | 16.58 | 0.61 | 76.79 | 47.6 | 0 | 21.17 | 15.83 | 14.16 | 9.71 | 6.72 | 2.91 |
| MnO | 0.69 | 0.28 | 0 | 0.29 | 0.33 | 0 | 0.21 | 0.19 | 0.12 | 0.20 | 0.22 | 0.05 |
| MgO | 11.23 | 11.07 | 0 | 1.19 | 2.1 | 0 | 11.33 | 4.07 | 3.53 | 2.25 | 1.49 | 0.59 |
| CaO | 22.48 | 11.08 | 6.75 | 0 | 0 | 55.8 | 0.1 | 10.45 | 8.90 | 5.79 | 3.84 | 1.53 |
| $Na_2O$ | 0.6 | 1.91 | 6.56 | 0 | 0 | 0 | 0.07 | 3.59 | 4.09 | 3.51 | 3.51 | 3.13 |
| $K_2O$ | 0 | 0.81 | 1.01 | 0 | 0 | 0 | 9.25 | 0.66 | 0.99 | 2.85 | 3.88 | 5.33 |
| $P_2O_5$ | 0 | 0 | 0 | 0 | 0 | 44.2 | | 1.58 | 1.69 | 0.88 | 0.58 | 0.17 |

| | mineral fractions $X_i$ in cumulates | | | | | | | |
|---|---|---|---|---|---|---|---|---|
| | Cpx | Hbl | Pl | Mgt | Ilm | Ap | Bt | Error |
| c1 | 0.125 | 0.222 | 0.471 | 0.117 | 0.029 | 0.036 | 0 | $\Sigma r^2 = 0.013$ |
| c2 | 0 | 0.281 | 0.541 | 0.108 | 0.009 | 0.038 | 0.024 | $\Sigma r^2 = 0.047$ |

[§] After Bogaerts *et al.* (2003). (*) experimentally determined composition of mineral (Bogaerts *et al.* 2003). Cumulates are made up of minerals in $X_i$ fractions; c1 is subtracted from liquid VDA9925 to give VDA9926, and c2 is subtracted from VDA9926 to give VDA9927, with an approximation of $\Sigma r^2$.

## Conclusions

The 1.5 Ga HBG suite, a major constituent of the Mazury Complex, is metaluminous and ferroan, and the felsic rocks are potassic A-type granitoids. The rocks thus belong to the AMCG suite with the particularity that they have crystallized in oxidized conditions. They were emplaced at pressures of *ca*. 2–5 kbar. The granitoids are associated with diorites, which crystallized from melts laden with cumulus minerals. The geochemical variations of these rocks define trends specific for each intrusion and corresponding to various batches of magma. The latter stretch along an overall trend, which mimics the Tranevåg liquid line of descent, a series formed by fractional crystallization of an oxidized and hydrous magma. Owing to the lack of Archean crust in this part of the East European Craton, the negative $\varepsilon_{Nd}$ at the time of intrusion (–3.3 to –4.7) and the relatively low Sr isotope initial ratios (0.702 to 0705) can be best explained by melting of a juvenile protolith ranging in age between 2.0 and 2.2 Ga. The Mazury oxidized A-type granitoids are spatially and temporarily associated with massif-type anorthosite and related reduced rocks. This is further evidence that different sources can be melted at the same time to provide parental magmas of different $H_2O$ contents. The Mazury Complex intruded a mega-linear discontinuity in the lithosphere along which delamination could provide the necessary heat of melting.

## Acknowledgements

This paper is dedicated to the memory of Ron Emslie. Ron was an outstanding scientist, an excellent field geologist and a brilliant petrologist. He developed in 1980 a paradigmatic model of evolution of the AMCG suite, still to be disproved. We owe him three decades of fruitful debates, particularly during decisive field trips in Proterozoic provinces all over the world. B.B. has benefitted from a grant of the Belgian CGRI to support periods of work at the University of Liège. B.B and J.W. have been supported by the Polish NCSR grants 6.20.9316.00.0, 3P04D01423 and 2P04D05527. P. Dzierżanowski, L. Jeżak. I. Iwasińska-Budzyk (Warsaw), G. Bologne (Liège), and C. Bosq (Clermont-Ferrand) are warmly acknowledged for their assistance with chemical analyses. We are grateful for the reviews of J.B. Whalen and G. Markl, as well as the editorial handling of J. Scoates.

## References

Anderson, J.L. & Bender, E.E. (1989): Nature and origin of Proterozoic A-type granitic magmatism in the southwestern United States of America. *Lithos* **23**, 19-52.

Anderson, J.L. & Morrison, J. (2005): Ilmenite, magnetite, and peraluminous Mesoproterozoic anorogenic granites of Laurentia and Baltica. *Lithos* **80**, 45-60.

ASHWAL, L.D. (1993): *Anorthosites*. Springer, Berlin, Germany.

BAGINSKI, B., DUCHESNE, J.-C., MARTIN, H. & WISZNIEWSKA, J. (2001a): Mid-Proterozoic granitoids from the Mazury Complex (NE Poland): AMCG Affinities? *EUG XI, J. Conf. Abstr.* **6**, 768.

BAGINSKI, B., DUCHESNE, J.-C., MARTIN, H. & WISZNIEWSKA, J.G. (2007): Isotopic and geochemical constraints on the evolution of the Mazury granitoids, NE Poland. *In* Granitoids in Poland (A. Koslowsly & J. Wiszniewska, eds.). AM Monograph **1**, 11-30.

BAGINSKI, B., DUCHESNE, J.-C., VANDER AUWERA, J., MARTIN, H. & WISZNIEWSKA, J. (2001b): Petrology and geochemistry of rapakivi-like granites from the crystalline basement of NE Poland. *Geol. Quart.* **45**, 33-52.

BOGAERTS, M., SCAILLET, B., LIÉGEOIS, J.-P. & VANDER AUWERA, J. (2003): Petrology and geochemistry of the Lyngdal granodiorite (southern Norway) and the role of fractional crystallization in the genesis of the Proterozoic ferro-potassic A-type granites. *Precamb. Res.* **124**, 149-184.

BOGAERTS, M., SCAILLET, B. & VANDER AUWERA, J. (2006): Phase equilibria of the Lyngdal granodiorite (Norway): implications for the origin of the metaluminous ferroan granitoids. *J. Petrol.* **47**, 2405-2431.

BOGDANOVA, S. (1999): The Palaeoproterozoic terrane pattern in the western part of the East European craton. Seventh EUROBRIDGE Workshop: Between EUROBRIDGE and TESZ. Polish Geological Institute, Suwalki-Szelment, Poland, 111-113.

BOGDANOVA, S., GORBATSCHEV, R., GRAD, M., JANIK, T., GUTERCH, A., KOZLOVSKAYA, E., MOTUZA, G., SKRIDLAITE, G., STAROSTENKO, V.I., TARAN, L. & E.A.P.W. GROUPS (2006): EUROBRIDGE: new insight into the geodynamic evolution of the East European Craton. *In* European Lithosphere Dynamics (D.G. Gee & R. Stephenson, eds.). *Geol. Soc. London, Mem.* **32**, 569-625.

BOGDANOVA, S., PASHKEVICH, I.K., BURYANOV, V.B., MAKARENKO, I.B., ORLYUK, M.I., SKOBELEV, V.M., STAROSTENKO, V.I. & LEGOSTAEVA, O.V. (2004): The 1.80–1.74 Ga anorthosite – rapakivi granite Korosten Pluton in the Ukrainian Shield: a 3-D geophysical reconstruction of deep structure. *Tectonophysics* **381**, 5-27.

CLAESSON, S., BOGDANOVA, S.V., BIBIKOVA, E.V. & GORBATSCHEV, R. (2001): Isotopic evidence of Paleoproterozoic accretion in the basement of the East European Craton. *Tectonophysics* **339**, 1-18.

CLAESSON, S. & RYKA, W. (1999): Nd model ages of the Precambrian crystalline basement of NE Poland. *In* Between EUROBRIDGE and TESZ. 7th EUROBRIDGE Workshop (Suwalki, Poland), 17-19.

CLAESSON, S., SUNDBLAD, K., RYKA, W. & MOTUZA, G. (1995): The Mazury Complex – an extension of the Transscandinavian igneous belt (TIB) into East European Platform? *Terra Abstract Suppl.* **7**, 107.

COCHERIE, A. (1986): Systematic use of trace element distribution patterns in log–log diagrams for plutonic rocks. *Geochim. Cosmochim. Acta* **50**, 2517-2522.

DALL'AGNOL, R., LAFON, J.-M. & MACAMBIRA, M.J.B. (1994): Proterozoic anorogenic magmatism in the Central Amazonian province, Amazonian Craton: geochronological, petrological and geochemical aspects. *Mineral. Petrol.* **50**, 113-138.

DALL'AGNOL, R., SCAILLET, B. & PICHAVANT, M. (1999): An experimental study of a lower Proterozoic A-type granite from the Eastern Amazonian craton, Brazil. *J. Petrol.* **40**, 1673-1698.

DEPAOLO, D.J. (1983): Geochemical evolution of the crust and mantle. *Rev. Geophys. Space Phys.* **21**, 1347-1358.

DE WIT, M.J., BOWRING, S.A., ASHWAL, L.D., RANDRIANASOLO, L.G., MOREL, V.P.I. & RAMBELOSON, R.A. (2001): Age and tectonic evolution of Neoproterozoic ductile shear zones in southwestern Madagascar, with implications for Gondwana studies. *Tectonics* **20**, 1-45.

DUCHESNE, J.-C. (1990): Origin and evolution of monzonorites related to anorthosites. *Schweiz. Mineral. Petrogr. Mitt.* **70**, 189-198.

DUCHESNE, J.-C., LIÉGEOIS, J.-P., VANDER AUWERA, J. & LONGHI, J. (1999): The crustal tongue melting model and the origin of massive anorthosites. *Terra Nova* **11**, 100-105.

DUCHESNE, J.-C., VANDER AUWERA, J., LIÉGEOIS, J.-P., BARTON, E.S. & CLIFFORD, T.N. (2007): Geochemical contraints on the petrogenesis of the O'okiep Koperberg Suite and granitic plutons in Namaqualand, South Africa: a lower crustal mafic source in Namaquan (Grenville) times. *Precamb. Res.* **153**, 116-142.

DUCHESNE, J.-C. & WILMART, E. (1997): Igneous charnockites and related rocks from the Bjerkreim–Sokndal layered intrusion (southwest Norway): a jotunite (hypersthene monzodiorite)-derived A-type granitoid suite. *J. Petrol.* **38**, 337-369.

DÖRR, W., BELKA, Z., MARHEINE, D., SCHASTOK, J., VALVERDE-VAQUERO, P. & WISZNIEWSKA, J. (2002): U–Pb and Ar–Ar geochronology of anorogenic granite magmatism of the Mazury complex, NE Poland. *Precamb. Res.* **119**, 101-120.

EMSLIE, R.F. (1991): Granitoids of rapakivi granite – anorthosite and related associations. *Precamb. Res.* **51**, 173-192.

EMSLIE, R.F., HAMILTON, M.A. & THÉRIAULT, R.J. (1994): Petrogenesis of a Mid-Proterozoic anorthosite – mangerite – charnockite – granite (AMCG) complex: isotopic and chemical evidence from the Nain plutonic suite. *J. Geol.* **102**, 539-558.

Ewart, A. & Griffin, W.L. (1994): Application of proton microprobe data to trace-element partitioning in volcanic rocks. *Chem. Geol.* **117**, 251-284.

Frost, B.R., Barnes, C.G., Collins, W.J., Arculus, R.J., Ellis, D.J. & Frost, C.D. (2001): A geochemical classification for granitic rocks. *J. Petrol.* **42**, 2033-2048.

Frost, C.D. & Frost, B.R. (1997): Reduced rapakivi-type granites: the tholeiite connection. *Geology* **25**, 647-650.

Frost, C.D., Frost, B.R., Bell, J.M. & Chamberlain, K.R. (2002): The relationship between A-type granites and residual magmas from anorthosite: evidence from the northern Sherman batholith, Laramie Mountains, Wyoming, USA. *Precamb. Res.* **119**, 45-71.

Goldstein, S.L., O'Nions, R.K. & Hamilton, P. (1984): A Sm–Nd isotopic study of atmospheric dusts and particulates from major river systems. *Earth Planet. Sci. Lett.* **70**, 221-236.

Goodge, J.W. & Vervoort, J.D. (2006): Origin of Mesoproterozoic A-type granites in Laurentia: Hf isotope evidence. *Earth Planet. Sci. Lett.* **243**, 711-731.

Harrison, T.M. & Watson, E.B. (1984): The behavior of apatite during crustal anatexis: equilibrium and kinetic considerations. *Geochim. Cosmochim. Acta* **48**, 1467-1477.

Henderson, P. (1982): *Inorganic Geochemistry*. Pergamon Press, Oxford, U.K.

Hoffman, P.F. (1989): Speculations on Laurentia's first gigayear (2.0 to 1.0 Ga). *Geology* **17**, 135-138.

Jacobsen, S.B. & Wasserburg, G.J. (1980): Sm–Nd isotopic composition of chondrites. *Earth Planet. Sci. Lett.* **50**, 139-155.

Johnson, M. & Rutherford, M.J. (1989): Experimental calibration of the aluminum-in-hornblende geobarometer with application to Long Valley caldera (California) volcanic rocks. *Geology* **17**, 837-841.

Juskowiak, O. (1998): Occurrence, structure and mineral diversity of rocks from the Suwalki anorthosite massif. *In* Geology of the Sulwaki Anorthosite Massif (Northern Poland) (W. Ryka & M. Podemska, eds.). *Prace Panstwowego Instytutu Geologicznego* **161**, 53-80.

Kubicki, S. & Ryka, W. (1982): *Geological Atlas of Crystalline Basement in Polish part of East European Platform*. Wydawnictwa Geologiczne, Warsaw, Poland.

Leake, B.E. and 21 others (1997): Nomenclature of amphiboles: report of the Subcommittee on Amphiboles of the International Mineralogical Association, Commission on New Minerals and Mineral Names. *Can. Mineral.* **35**, 219-246.

Longhi, J. (2005): A mantle or mafic crustal source for Proterozoic anorthosites? *Lithos* **83**, 183-198.

Longhi, J., Vander Auwera, J., Fram, M.S. & Duchesne, J.-C. (1999): Some phase equilibrium constraints on the origin of Proterozoic (massif) anorthosites and related rocks. *J. Petrol.* **40**, 339-362.

Martin, H. (1987): Petrogenesis of Archaean trondhjemites, tonalites and granodiorites from eastern Finland: major and trace element geochemistry. *J. Petrol.* **28**, 921-953.

Martin, H., Bonin, B., Capdevila, R., Jahn, B.M., Lameyre, J. & Wang, Y. (1994): The Kuiqi peralkaline granitic complex (SE China): petrology and geochemistry. *J. Petrol.* **35**, 983-1015.

Morgan, J.W., Stein, H.J., Hannah, J.L., Markey, R.J. & Wiszniewska, J. (2000): Re–Os study of Fe-Ti-V oxide and Fe-Cu-Ni sulfide deposits, Suwalki anorthosite massif, northeast Poland. *Mineral. Deposita* **35**, 391-401.

Nelson, B.K. & DePaolo, D.J. (1985): Rapid production of continental crust 1.7 to 1.9 b.y. ago: Nd isotopic evidence from the basement of the North American mid-continent. *Geol. Soc. Am., Bull.* **96**, 746-754.

Peccerillo, R. & Taylor, S.R. (1976): Geochemistry of Eocene calc-alkaline volcanic rocks from the Kastamonu area, northern Turkey. *Contrib. Mineral. Petrol.* **58**, 63-81.

Pouchou, J.L. & Pichoir, J.F. (1991): Quantitative analysis of homogeneous or stratified microvolume applying the model "PAP". *In* Electron Probe Quantitation (K.F.J. Heinrich & D.E. Newbury, eds.). Plenum Press, New York, N.Y. (31-75).

Rollinson, H. (1993): *Using Geochemical Data: Evaluation, Presentation, Interpretation*. Longman Scientific and Technical, New-York.

Ryka, W. & Podemski, M. (1998): *Geology of the Suwalki anorthosite massif (Northern Poland)*. Prace Panstwowego Instytutu Geologicznego **161**, Warsaw, Poland.

Rämö, O.T., Dall'Agnol, R., Macarimba, M.J.B., Leite, A.A.S. & de Oliveira, D.C. (2002): 1.88 Ga oxidized A-type granites of the Rio Maria Region, eastern Amazonian Craton, Brazil: positively anorogenic! *J. Geol.* **110**, 603-610.

Rämö, O.T. & Haapala, I. (1995): One hundred years of rapakivi granite. *Mineral. Petrol.* **52**, 129-185.

Schmidt, M.W. (1992): Amphibole composition in tonalite as a function of pressure: an experimental calibration of the Al-in-hornblende barometer. *Contrib. Mineral. Petrol.* **110**, 304-310.

Scoates, J.S. & Chamberlain, K.R. (1997): Orogenic to post-orogenic origin for the 1.76 Ga Horse Creek anorthosite complex, Wyoming, USA. *J. Geol.* **105**, 331-343.

Skridlaite, G., Whitehouse, M. & Rimša, A. (2007): Evidence for a pulse of 1.45 Ga anorthosite – mangerite – charnockite – granite (AMCG) plutonism in Lithuania:

implications for the Mesoproterozoic evolution of the East European Craton. *Terra Nova* **19**, 294-301.

SKRIDLAITE, G., WISZNIEWSKA, J. & DUCHESNE, J.-C. (2003): Ferro-potassic A-type granites and related rocks in NE Poland and S Lithuania: west of the East European Craton. *Precamb. Res.* **124**, 305-326.

SUN, S.S. & MCDONOUGH, W.F. (1989): Chemical and isotopic systematices of oceanic basalts: implications for mantle composition and processes. *In* Magmatism in Ocean Basins (A.D. Saunders & M.J. Norry, eds.). *Geol. Soc., Spec. Publ.* **42**, 313-345.

TEYSSIER, C. & TIKOFF, B. (1998): Strike-slip partitioned transpression of the San Andreas fault system: a lithospheric-scale approach. *In* Continental Transpressional and Transtensional Tectonics (R.E. Holdworth, R.A. Strachan & J.F. Dewey, eds.). *Geol. Soc., Spec. Publ.* **135**, 143-158.

TOPLIS, M. & CARROLL, M.R. (1995): An experimental study of the influence of oxygen fugacity on Fe–Ti oxide stability, phase relations, and mineral–melt equilibria in ferrobasaltic systems. *J. Petrol.* **36**, 1137-1170.

VANDER AUWERA, J., BOGAERTS, M., BOLLE, O. & LONGHI, J. (2008): Genesis of intermediate igneous rocks at the end of the Sveconorwegian (Grenvillian) orogeny (S. Norway) and their contribution to intracrustal differentiation. *Contrib. Mineral. Petrol.* **156**, 721-743.

VANDER AUWERA, J., BOGAERTS, M., LIÉGEOIS, J.-P., DEMAIFFE, D., WILMART, E., BOLLE, O. & DUCHESNE, J.-C. (2003): Derivation of the 1.0–0.9 Ga ferro-potassic A-type granitoids of southern Norway by extreme differentiation from basic magmas. *Precamb. Res.* **124**, 107-148.

VANDER AUWERA, J., BOLOGNE, G., ROELANDTS, I. & DUCHESNE, J.-C. (1998a): Inductively coupled plasma-mass spectrometry (ICP–MS) analysis of silicate rocks and minerals. *Geologica Belgica* **1**, 49-53.

VANDER AUWERA, J., LONGHI, J. & DUCHESNE, J.-C. (1998b): A liquid line of descent of the jotunite (hypersthene monzodiorite) suite. *J. Petrol.* **39**, 439-468.

VIGNERESSE, J.L. (2007): The role of discontinuous magma inputs in felsic magma and ore generation. *Ore Geol. Rev.* **30**, 181-216.

WATSON, E.B. & HARRISON, T.M. (1983): Zircon saturation revisited: temperature and compositional effects in a variety of crustal magma types. *Earth Planet. Sci. Lett.* **64**, 295-304.

WATSON, E.B. & GREEN, T.H. (1981): Apatite/liquid partition coefficients for the rare earth elements and strontium. *Earth Planet. Sci. Lett.* **56**, 405-421.

WHALEN, J.B., CURRIE, K.L. & CHAPPELL, B.W. (1987): A-type granites: geochemical characteristics, discrimination and petrogenesis. *Contrib. Mineral. Petrol.* **95**, 407-419.

WISZNIEWSKA, J., CLAESSON, S., STEIN, H.J., VANDER AUWERA, J. & DUCHESNE, J.-C. (2002): The north-eastern Polish anorthosite massifs: petrological, geochemical and isotopic evidence for a crustal derivation. *Terra Nova* **14**, 451-460.

WISZNIEWSKA, J., WYBRANIEC, S. & BOGDANOVA, S. (2000): Combined geological and geophysical characteristics of AMCG complexes in NE Poland. *In* Transbaltic Precambrian Correlations. Field conference in the framework of the VISBY PROGRAMME and the EUROBRIDGE project, (Bornholm–Blekinge), Abstr. Vol., 7-8.

*Received February 3, 2009, revised manuscript accepted June 24, 2010.*

APPENDIX 1. DESCRIPTION OF SAMPLES IN DRILL CORES

| Drill core | | Depth (m) | Rock type |
|---|---|---|---|
| Bartoszyce 1 | B1 | 2125 | Qtz monzodiorite |
| Bartoszyce 2 | B2 | 2127 | Qtz monzodiorite |
| Bartoszyce 3 | B3 | 2130.5 | Qtz monzonite |
| Bartoszyce 4 | B4 | 2133.5 | Qtz monzodiorite |
| Bartoszyce 5 | B5 | 2137 | Qtz monzodiorite |
| Bartoszyce 6 | B6 | 2142 | Diorite |
| Bartoszyce 7 | B7 | 2146 | Qtz monzonite |
| Filipów 1 | F1 | 1048 | Qtz monzodiorite |
| Filipów 2 | F2 | 1088 | Qtz monzodiorite |
| Filipów 3 | F3 | 1123 | Qtz monzonite |
| Filipów 4 | F4 | 1203 | Qtz monzodiorite |
| Filipów 5 | F5 | 1242 | Qtz monzodiorite |
| Filipów 6 | F6 | 1301.5 | Qtz monzodiorite |
| Filipów 7 | F7 | 1351.5 | Qtz monzodiorite |
| Filipów 8 | F8 | 1377 | Qtz monzodiorite |
| Filipów 9 | F9 | 1412 | Qtz monzodiorite |
| Filipów 10 | F10 | 1432 | Qtz monzodiorite |
| Filipów 11 | F11 | 1491.5 | Qtz monzodiorite |
| Filipów 13 | F13 | 1553 | Qtz monzodiorite |
| Filipów 14 | F14 | 1620 | Qtz monzodiorite |
| Filipów 15 | F15 | 1653 | Qtz monzodiorite |
| Gołdap 1 | G1 | 1635 | Granodiorite |
| Gołdap 1b | G1b | 1635.5 | Granodiorite |
| Gołdap 2 | G2 | 1638 | Granite |
| Gołdap 3 | G3 | 1645 | Qtz monzonite |
| Gołdap 4 | G4 | 1648 | Qtz monzonite |
| Gołdap 5 | G5 | 1651 | Granodiorite |
| Gołdap 6 | G6 | 1654 | Granodiorite |
| Gołdap 7 | G7 | 1657 | Granodiorite |
| Gołdap 8 | G8 | 1660 | Qtz monzonite |
| Kętrzyn 1 | K1 | 1535 | Qtz syenite |
| Kętrzyn 3 | K3 | 1541.5 | Monzodiorite |
| Kętrzyn 4 | K4 | 1546.5 | Monzodiorite |
| Kętrzyn 5 | K5 | 1549.5 | Monzodiorite |
| Kętrzyn 6 | K6 | 1553.5 | Monzodiorite |
| Kętrzyn 7 | K7 | 1558 | Qtz monzodiorite |
| Klewno 1 | KW1 | 1782 | Diorite |
| Klewno 2 | KW2 | 1785 | Diorite |
| Klewno 3 | KW3 | 1788 | Diorite |
| Klewno 4 | KW4 | 1792.5 | Diorite |
| Klewno 5 | KW5 | 1797.5 | Diorite |
| Pawłówka 17 | P17 | 1822 | Qtz monzodiorite |
| Pawłówka 144 | P144 | 1879 | Qtz monzodiorite |

Coordinates of drill holes: Bartoszyce: 54°14'07", 20°57'03"; Filipów: 54°12'14", 22°36'22"; Gołdap: 54°16'59", 22°07'29"; Kętrzyn: 54°10'23", 21°02'45", Klewno: 54°04'29", 21°10'20"; Pawłówka: 54°12'20", 22°47'33".